

Copyright
by
Revanth Bodepudi
2019

**The Thesis Committee for Revanth Bodepudi
Certifies that this is the approved version of the following thesis:**

Elastic Behavior of the Germanium Nanowire Membrane

**APPROVED BY
SUPERVISING COMMITTEE:**

Kenneth M. Liechti, Supervisor

Rui Huang

Elastic Behavior of the Germanium Nanowire Membrane

by

Revanth Bodepudi

Thesis

Presented to the Faculty of the Graduate School of

The University of Texas at Austin

in Partial Fulfillment

of the Requirements

for the Degree of

Master of Science in Engineering

The University of Texas at Austin

May 2019

Acknowledgements

I wish to sincerely thank my advisor Dr. Kenneth M. Liechti for giving me the opportunity to work under his guidance during my graduate study at the University of Texas at Austin. I have learned a lot from his experience and enjoyed working with him. I also want to express my gratitude for his help and guidance on my research, coursework throughout these two years. I want to thank Dr. Rui Huang for not only taking the time to read this thesis but also for providing me regular feedback and guidance on my research.

I wish to thank Joe from the machine shop and Pablo from the electronics shop. Joe helped me fabricate some parts for the experiment setup. He went above and beyond to deliver most of the parts on time with high precision, and I am very grateful for this. Pablo was also always here to help on electronics issues.

I thank the University of Texas at Austin, the Aerospace Engineering & Engineering Mechanics department and the Material Research Science and Engineering Center which financed my studies and research.

I also owe special thanks to my friends whom I cannot list one by one for fear of missing some of them out. In difficult times, these were ones I looked to for the courage to push through. For the joy, support and the long-lasting memories I will cherish forever, my deepest regards and thanks.

Finally, my parents Kiran and Nirmala to whom I owe everything in life and career. From childhood they instilled in me a love for learning and knowledge, aspects I carry to this day and beyond. For giving me the freedom to pursue my goals, thank you.

Abstract

Elastic Behavior of the Germanium Nanowire Membrane

Revanth Bodepudi, M.S.E

The University of Texas at Austin, 2019

Supervisor: Kenneth M. Liechti

Semiconductor nanowires promise to provide the building blocks for a new generation of nanoscale devices. Recently, researchers have worked on developing new membranes out of semiconductor nanowires. Due to its small dimensions and porous network structure, obtaining the mechanical properties of these membranes is very challenging. This work presents a bulge test method for determining the mechanical properties of the porous germanium nanowire membrane. Theoretical bulge equations for circular and rectangular shaped samples were derived. A parametric analysis was conducted to determine the optimum configuration and guide the selection of components for the apparatus. A laminate comprising the germanium nanowire membrane and a polymer film was fabricated due to the porosity of the nanowire membrane. The bulge test apparatus was designed and developed to test circular and rectangular shaped composite samples that are required to extract Young's modulus and Poisson's ratio. The Young's modulus and the Poisson's ratio of the germanium nanowire membrane were found to be 208 MPa and 0.10, respectively.

Table of Contents

List of Tables	viii
List of Figures	ix
CHAPTER 1: INTRODUCTION	1
1.1 THIN FILM TEST METHODS	4
Thermal cycling of film on substrates	5
Nanoindentation.....	6
Micro-tensile test	6
Bulge Test	7
CHAPTER 2: ANALYSIS	11
2.1 Bulge equation	11
2.1.1 Circular Profile.....	12
2.1.2 Rectangular profile.....	18
2.1.3 Extraction of mechanical properties	23
2.2 Parametric Study.....	25
2.2.1 Pressure selection.....	26
2.2.2 Polymer selection.....	29
2.2.3 Thickness selection	31
CHAPTER 3: EXPERIMENT	37
3.1 Apparatus	37
3.1.1 Manifold.....	38
3.1.2 Pressure System	40
Pressure Generation	40

Pressure Detection	43
Pressure Calibration	46
3.1.2 Deflection system.....	48
Deflection Measurement	48
Deflection Calibration.....	51
3.2 Material Preparation	54
3.2.1 Germanium Nanowire Synthesis	54
Materials	54
Procedure	55
3.2.2 PET Film.....	56
3.2.3 Specimen.....	58
3.3 Experiment Procedure.....	63
CHAPTER 4: RESULTS	65
Data Analysis	65
CHAPTER 5: CONCLUSION	71
Further Work.....	72
References.....	74

List of Tables

Table 2.1: Summary of bulge equations for different sample geometries used in the bulge test experiment for extracting its mechanical properties	23
Table 2.2: Bulge test design parameters.....	25
Table 2.3: Design parameter range of values for polymers (ref. CES Edu pack)	27
Table 2.4: Chosen design parameter value (polymers) for the parametric analysis.....	27
Table 2.5: Required bulge pressure range for each polymer.....	28
Table 2.6: Parametric analysis using error determination technique for polymer selection (units of the elastic modulus are given in Pa).....	30
Table 2.7: Parametric analysis for polymer thickness selection (units of the elastic modulus are given in Pa).....	32
Table 2.8: Chosen design parameter values from the parametric study.....	36
Table 3.1: Pixel and length measurement values for calibration	51

List of Figures

Figure 2.1: Cross-section of the bulged sample model; indicating the design parameters	12
Figure 2.2: Isometric view of the bulged circular sample model.....	12
Figure 2.3: Schematic diagram showing the relation between geometric parameters of the circular bulge sample	13
Figure 2.4: Thin-walled half sphere model subjected to uniform pressure (P).....	14
Figure 2.5: Schematic diagram of the bulged rectangular sample	18
Figure 2.6: Sketch indicating aspect ratio and shape deviation effect ⁵¹ of the rectangular sample	18
Figure 2.7: Thin-walled half cylinder model subjected to uniform pressure (P).....	19
Figure 2.8: Schematic diagram showing the relation between geometric parameters of the rectangular bulge sample	20
Figure 2.9: Cross-sectional schematic diagram of the composite deposited on the substrate with an orifice	25
Figure 3.1: Manifold	39
Figure 3.2: Syringe pump and valve block	41
Figure 3.3: Stepper motor and control box	41
Figure 3.4: Schematic diagram of the pressure generation system.....	42
Figure 3.5: Various connections to the manifold.....	43
Figure 3.6: Signal conditioner and voltmeter.....	44
Figure 3.7: Schematic diagram of the pressure detection system	45
Figure 3.8: Plot showing the pressure vs voltage relation	47
Figure 3.9: Digital camera on positioner and light source	49

Figure 3.10: Schematic diagram of the deflection measurement system.....	50
Figure 3.11: Bulge test experiment set-up	53
Figure 3.12: Schematic diagram of the supercritical fluid-liquid-solid (SFLS) nanowire growth reactor system	55
Figure 3.13: LPKF Protolaser cutting machine	57
Figure 3.14: circular PET samples cut (OD-30mm).....	58
Figure 3.15: Concentric circular double-sided tape (OD-30mm, ID- 10mm)	59
Figure 3.16: PET film attached to the substrate with circular orifice	59
Figure 3.17: Concentric rectangular double-sided tape (OD-30mm, ID- 20mm*4mm) ..	60
Figure 3.18: PET film attached to the substrate with rectangular orifice	61
Figure 3.19: Spray coating machine	61
Figure 3.20: Composite (Ge-NW membrane deposited on PET) on the substrate:.....	62
Figure 3.21: SEM image of the spray coated sample	63
Figure 4.1: Pressure vs Deflection plot for the 13micron PET film from the bulge test ..	66
Figure 4.2: Pressure vs Deflection plot for the 18micron circular composite sample from the bulge test	67
Figure 4.3: Pressure vs Deflection plot for the 18micron rectangular composite sample from the bulge test	68

CHAPTER 1: INTRODUCTION

Nanoscale materials are of great interest because of the possibilities they offer for obtaining new properties at a small size. When structures approach the ~100 nm size regime, their properties may change with decreasing size for the same atomic composition. This size dependence derives from three primary effects:

1. The ratio of surface area to volume becomes larger, with surface atoms having higher energy and different coordination.
2. Interfaces between nanostructures become a significant component of the structures, with their modified electronic properties, strain gradients, and influence on the flow of defects, charge carriers, and phonons.
3. Sufficiently reduced dimensions lead to quantum size effects and coherent interactions between structures.

These size-dependent effects result in changes in the physical properties of nanomaterials as well as changes in the interaction of electromagnetic energy and transport of energy through nanomaterials. One-dimensional (1-D) structures such as nanowires provide a particularly attractive class of nanomaterials. One can tailor the functionality of nanowires in a variety of ways, and their geometry is optimal for achieving new regimes of 1-D transport of charge carriers and heat to realize new devices.

Semiconducting nanowires are particularly versatile because of the wide range of properties that can be achieved. Thus, much attention has been focused on these structures and their potential applications in areas such as electronic^{1-4,23,24} and photonic devices^{15,25}, chemical and biomolecular sensing^{6,7}, and energy harvesting and storage^{21,25}. Synthetic advances to achieve high-quality nanowires with control over size and size dispersity,

composition, phase, and physical properties have further driven progress toward applications. Among the many exciting properties of quantum wires are their size and shape dependent bandgap energies¹⁻⁵, polarization anisotropies⁶⁻⁹, large absorption cross sections¹⁰⁻¹², and one-dimensional charge transport^{13,14}. Besides, their charge-carrier dynamics has a practical importance¹⁵⁻¹⁸ and may enable devices for solar-energy conversion, electronics, and LEDs.

Germanium is one of the best semiconductors due to its high electron and hole mobilities of 3800 and 1820 $cm^2V^{-1}s^{-1}$ respectively. It also possesses an ultrahigh theoretical specific capacity of 1384 $mAh g^{-1}$. Nanowires made of germanium are of high interest for electronic applications due to the one-dimensional charge-transport property they possess. Due to its high electron mobility, germanium nanowires are one of the best material for high-performance field-effect transistors^{19,20}.

Due to its high specific capacity, which is much higher than that of graphite (372 $mAh g^{-1}$), the next-generation Lithium-ion batteries^{21,22} can use germanium nanowires as an electrode material. From the perspective of electron transport, germanium nanowires are of particular interest due to the continuous transport path along the wire length. Additionally, the thin diameters of nanowires significantly reduce the diffusion paths for Li ions²¹, which is critically important for enhancing rate capabilities. Various advantages of germanium nanowires make it one of the most important materials for applications in electronics^{23,24}, energy storage²⁵ and solar-energy conversion^{24,26}.

Various researchers have actively explored synthesizing and obtaining the material properties of germanium nanowires. The Korgel group measured the mechanical properties of Supercritical Fluid-Liquid-Solid grown germanium nanowires by bending each with a robotic nanomanipulator in a scanning electron microscope (SEM)²⁷. The nanowires tolerated a diameter-dependent flexural strain of up to 17% prior fracture, which is two

orders of magnitude higher than bulk Ge. The bending strength was observed to be 18 GPa and agrees with the ideal strength of 14-20 GPa for a perfect Ge- crystal. Realizing the potential of Supercritical Fluid-Liquid-Solid grown germanium nanowires, The Korgel and Freeman groups further worked on developing nanowire aerogels and nanowire membranes, respectively.

Aerogel is a synthetic porous ultralight material derived from a gel, in which the gas replaces the liquid component of the gel. The result is a solid with extremely low density and low thermal conductivity. Germanium nanowire aerogels have a porous solid network that contains air pockets, with the air pockets taking up the majority of space within the material: a nanowire network structure with 99% air.

A membrane is a selective barrier which allows some things to pass through but stops others. Germanium nanowire membranes developed in the Freeman group are porous network layers which reject particles larger than 0.005 μm . Ultrafiltration and nanofiltration are some of the potential applications for the germanium nanowire membrane.

Filtration requires the membrane to withstand a certain amount of pressure/force. To develop the germanium nanowire membrane for its application in ultrafiltration and nanofiltration, understanding the mechanical properties of germanium nanomembrane is highly desired. Besides, the mechanical properties of membranes may have a significant difference in them due to variations in processing conditions. The temperature, humidity, or the order of fabrication procedures may induce a significant difference in the parameters governing properties. Characterization of the elastic mechanical properties such as Young's modulus and Poisson's ratio is often found to be necessary to increase the reliability and control the costs.

Existing methods for obtaining the mechanical properties of large scale materials cannot be directly applicable to membranes. The thickness of a germanium membrane is in the range of 100 nanometers to few micrometers; thus, membranes are analogous to thin films. In the last century, various techniques and testing methods were developed for characterizing the mechanical properties of thin films. These techniques and test methods are discussed in section 1.1 and the best test method to determine the mechanical properties of germanium nanowire membrane was chosen.

1.1 THIN FILM TEST METHODS

The behavior of materials in thin-film form often differs from that of their bulk counterparts²⁹. This difference is owing to the dimensional constraints and to the microstructure that develops during the growth of thin films. Therefore, it is not possible to extrapolate material properties from bulk to typical thin-film thicknesses in the range 10 nm–10 μ m.

For example, thin metal films are often found to support much higher stresses than the same material in bulk form, and their yield stress is inversely proportional with the film thickness if the film surface is passivated^{30,31}. Besides the effects associated with film thickness, mechanical properties also depend strongly on film microstructure and fabrication process³².

Unfortunately, because of their small dimensions, the techniques commonly used to measure these properties in bulk materials are not directly applicable to thin films. As a result, several specialized testing techniques have been developed to study mechanical properties in small dimensions. As in macroscopic testing, the aim is to determine material

properties such as Young's modulus, strength, or fracture toughness. It requires new ways to measure stresses and strains in small volumes.

An overview of the most common techniques for mechanical testing of thin films²⁸ is given in the following sections. Among them, the substrate curvature and nanoindentation techniques are widely used and commercialized. The uniaxial micro-tensile test and the bulge test techniques are extensively used for measuring the mechanical behavior of freestanding thin films.

Thermal cycling of film on substrates

A common technique to characterize the mechanical behavior of a thin film on a substrate is to subject the film/substrate composite to a thermal cycle and monitor the stress evolution in the film either by measuring the substrate curvature or by x rays. This technique is particularly useful when there is a significant difference between the thermal expansion coefficients of film and substrate as, for instance, in the case of thin metal films on silicon or glass substrates (Nix³³).

Substrate curvature technique involves very little sample preparation since it directly tests thin films deposited on substrates. Strain and temperature cannot be varied independently in these experiments. As a result, the measured stresses in the film result from a convolution of the temperature dependence of the film strength, strain hardening, and recovery at elevated temperatures, thereby making it difficult to interpret the results and leading to errors in the measured data.

Nanoindentation

Nanoindentation is a depth-sensing indentation (DSI) technique³⁴ used to obtain mechanical properties from small volumes of material. In a traditional indentation test, an indenter is pressed into a sample with a known load and removed. The hardness is then defined as the load divided by the area of the residual indentation and gives a measure of the resistance of the material to plastic deformation. In DSI, the load on and displacement of the indenter are continuously recorded as it is pressed into and removed from the sample. These data are subsequently analyzed to determine mechanical properties. DSI data provide hardness, elastic modulus, strain rate sensitivity, and other properties.

Determination of the mechanical properties of new thin film materials on substrates by indentation has always been difficult because of the influence of the substrate on the measured properties. The indentation response of a thin film on a substrate is a complex function of the elastic and plastic properties of both the film and substrate, and it is also not suitable for measuring the work-hardening behavior or the residual stress in the film.

Micro-tensile test

For bulk materials, tensile testing is the most important technique for characterizing mechanical properties, because information on Young's modulus, ultimate tensile strength, and ductility can be obtained from a single experiment. For thin films, tensile testing is not as commonly used because the handling of freestanding thin-film specimens and measurement of strains in small dimensions are not easy. Both problems, however, have been overcome by developing specialized techniques. Read, and Dally³⁵ accomplished the processing of a thin-film specimen for tensile testing by using lithographical and etching techniques after film deposition onto a silicon substrate. After etching, the dog-bone-shaped freestanding film specimen is still supported by a silicon

frame, which allows the film to be mounted and aligned in the tensile tester without damaging it. Just before testing, the frame is cut using a diamond saw. For the strain measurement, it is not possible to attach a strain gauge to the sample, so several methods have been developed to measure the strain without contacting the sample including optical and electrical methods (Brotzen³⁶).

Due to difficulties associated with sample handling at the micron or submicron scale, micro-tensile testing often suffers from alignment and gripping problems. Although recent progress of Si micromachining techniques to fabricate tensile specimens has been made these methods yet are not so cost-effective.

Bulge Test

In the bulge test, freestanding thin films are obtained by opening an orifice in the substrate typically using micromachining techniques. The freestanding film is then deflected when a uniform pressure is applied to the film. The mechanical properties of the film are determined from its pressure-deflection behavior. The stress state in the film is biaxial so that only properties in the plane of the film were measured.

Compared with micro-tensile testing, the bulge test technique has the unique advantage of precise sample fabrication and minimal sample handling. With some care, freestanding films as thin as 1 nm films can be prepared and tested.

Bulge testing of thin films was first reported by Beams³⁷, as a technique for measuring in-plane mechanical properties of thin films. In the beginning, the test has been plagued by many problems. The results were rather sensitive to small variations of the dimensions of the film and may be affected by twisting of the sample when it is mounted. Sample preparation is therefore crucial, and individual steps need to be taken to minimize these effects.

The recent development of microfabrication technology has made it possible to manufacture bulge test samples with precisely controlled dimensions and has dramatically reduced sample handling. These improvements have made accurate bulge testing possible. To explain the experimental data and relate them to the mechanical properties of the tested films, both theoretical and numerical analyses have been conducted to understand the pressure–deflection relation for membranes with various shapes. Hencky³⁸ was the first to publish an analytical solution for the elastic deflection of a pressurized circular membrane with fixed edges.

Vlassak³⁹ generalized Hencky's solution to include the influence of residual stress on the deflection of a membrane. The problem becomes more complicated for noncircular geometries such as square or rectangular membranes. Levy⁴⁰ gave an exact elastic solution for the problem of a pressurized square membrane but is too complicated to be practically useful. Many researchers have developed approximate solutions using energy minimization methods.

Vlassak and Nix⁴¹ derived an accurate expression for the elastic load-deflection behavior of square and rectangular membranes following an approach initially developed by Timoshenko⁴². This expression also includes the effect of the residual stress on the membrane deflection. These researchers further found that once the aspect ratio of a rectangular membrane exceeds 4, the deflection at the center of the membrane is nearly independent of the aspect ratio and can be approximated with the exact solution for an infinitely long rectangular membrane, which can be readily derived⁴¹.

Many researchers analyzed the accuracy and reliability of the bulge test. Itozaki⁴³ showed that failure to include the initial height of the membrane in the analysis leads to an apparent nonlinear elastic behavior of the film. Vlassak et al.⁴¹ determined the Poisson's ratio by performing a bulge test on both square and rectangular membranes of the same

film. Small et al.^{44,45} analyzed the influence of initial film conditions such as film wrinkling, residual stress, and initial height of the membrane using finite element analysis. Vlassak³⁹ investigated the contribution of the film bending stiffness to the deflection of a membrane. He showed that for typical bulge test geometries, the bending moment is only significant very close to the edge of the membrane and is negligible everywhere else. Xiang⁴⁶ further verified the accuracy of the developed models in the plastic regime by conducting a plane-strain test.

These analyses, together with new sample preparation techniques, have made the bulge test a useful technique to accurately measure the elastic properties of both freestanding films and multilayers across a wide range of materials, including metals, polymers, and ceramics.

In summary, a bulge test eliminates the substrate influence and clamping problems associated with nanoindentation and micro-tensile tests respectively. It is a non-destructive and cost-effective method which requires minimal specimen handling and usually features a relatively simple and portable design. Bi-axial stress state of the sample in the bulge test helps in measuring the in-plane properties of the film. Thus, out of the techniques mentioned above, the bulge test is the most suitable for characterizing the mechanical properties of germanium nanowire membrane.

In the bulge test experiment, a uniform pressure applied to the Ge-NW membrane can cause pressure leaks in the system due to its porous membrane structure. A bi-layered material (composite) comprising a polymer and Ge-NW membrane is introduced to eliminate the pressure leaks. Uniform pressure is applied on the polymer side of the composite during the experiment.

In this report, the mechanical properties of germanium nanowire membrane are determined by performing the bulge test experiment. Derivation of the bulge equations and the parametric analysis to determine the suitable design parameters for the experiment are discussed in Chapter 2. The components used for developing the bulge test setup and the fabrication techniques utilized for preparing the sample are described in Chapter 3. The results of the mechanical properties of the Ge-NW membrane are presented in Chapter 4, followed by conclusions and recommendations for future work in Chapter 5.

CHAPTER 2: ANALYSIS

In this chapter, we derive the bulge equations showing the relation between the bulge test parameters and the mechanical properties of the sample, and we describe the parametric analysis conducted for developing the bulge test experiment setup.

The equations governing the determination of Young's modulus and Poisson's ratio depend on the shape of the sample. The bulge equations for circular and rectangular profiles and the extraction of mechanical properties of the sample are derived in section 2.1. A suitable range of values for the material and geometric design parameters determined from the parametric study are described in section 2.2.

2.1 BULGE EQUATION

In the bulge test, a uniform pressure is applied to the sample (film/membrane), and the resulting maximum central bulge deflection is observed. The bulge deflection is related to the strain experienced by the sample, while the applied pressure is related to the stress in the sample. Thus, the mechanical properties for a sample of a given material can be measured by obtaining the pressure-deflection relationship.

The geometric parameters involved in the bulge test method are the sample thickness, substrate orifice size, and orifice shape. Orifice size and orifice shape refer to the geometrical features of the cavity in the substrate whose boundaries define the sample dimension and shape subjected to the uniform pressure. The orifice size and orifice shape are critical because they define the strain state of the sample. Different deformation states can be studied by changing the orifice shape and orifice size. The essential parameters in the bulge test experiment are shown in Figure 2.1.

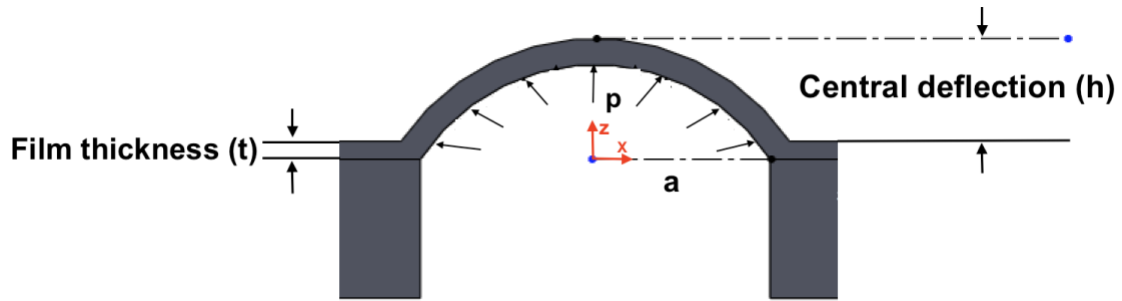


Figure 2.1: Cross-section of the bulged sample model; indicating the design parameters

Where p is the applied bulge pressure, t is the thickness of the sample, h is the maximum central bulge deflection, a is the orifice size.

2.1.1 Circular Profile

A circular orifice on the substrate results in a circular profile on the sample subjected to the applied pressure. A schematic of a bulged circular sample is shown in Figure 2.2.



Figure 2.2: Isometric view of the bulged circular sample model

For a pressurized circular profile, we can show that the bulged shape is parabolic and the radius of curvature (R) of the bulged sample can be calculated from the geometry of the cross-section of the specimen.

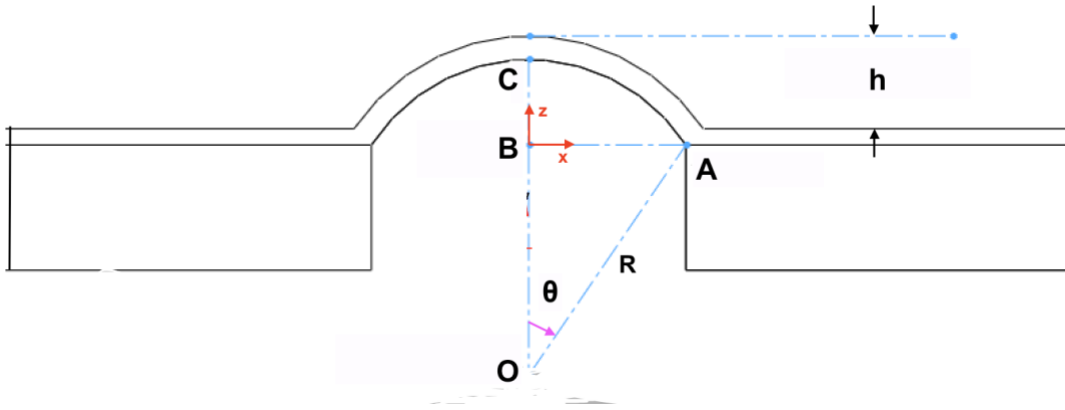


Figure 2.3: Schematic diagram showing the relation between geometric parameters of the circular bulge sample

Assuming the bulge deflection is symmetric about the z -axis, the geometric relation between the maximum deflection (h) and the radius of sample (a) is shown in Figure 2.3. For small deflections of the sample, the maximum central deflection is much less than the radius of the sample ($h \ll a$).

From the ΔOAB using Pythagoras theorem, a relation between the maximum deflection (h), sample radius (a) and radius of curvature of the sample (R) can be determined.

$$\begin{aligned}
 OA^2 &= OB^2 + AB^2 \\
 R^2 &= (R - h)^2 + a^2 \\
 \Rightarrow R^2 &= R^2 - 2Rh + h^2 + a^2 \\
 \Rightarrow 2Rh &= h^2 + a^2
 \end{aligned}$$

as $h \ll a$, h^2 is very small and can be neglected,

$$2Rh = a^2$$

The radius of curvature (R) of the bulged sample is

$$R = \frac{a^2}{2h} \quad (2.1)$$

The pressurized sample is modeled as a section of a thin-walled half sphere as shown in Figure 2.4 to determine the stress state in the bulged thin circular profile.

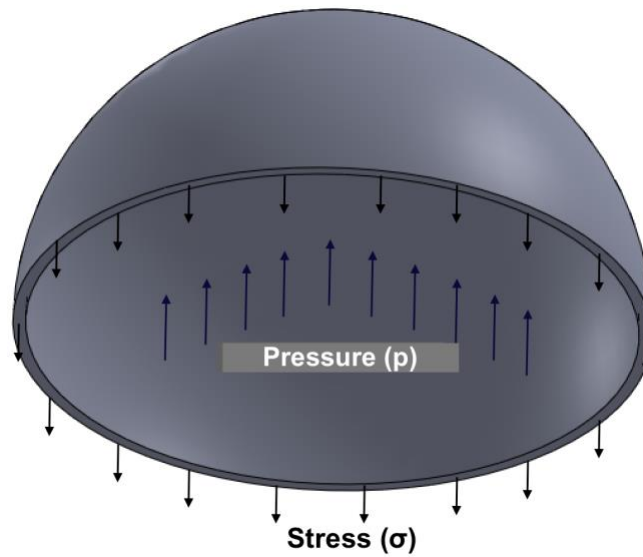


Figure 2.4: Thin-walled half sphere model subjected to uniform pressure (p)

In the spherical bulge model, the stress and strain are in-plane and equi-biaxial^{37, 47} ($\sigma_{xx} = \sigma_{yy} = \sigma = \sigma_r, \varepsilon_r = \varepsilon$). It is also called a plane-stress condition. Where σ_r and ε_r represent the stress and strain within the bulged sample in the radial direction respectively. Force equilibrium along the deflection direction; gives the radial stress as

$$\sigma_r = \frac{pR}{2t} \quad (2.2)$$

Equation (2.2) indicates the relation between the applied pressure (p), the radius of curvature (R), and radial stress on the bulged thin sample (σ_r).

The corresponding strain ϵ_r in the sample can be derived using the cross-section length of the sample before and after the bulge. From Figure 2.3,

$$\sin(\theta) = a/R$$

Initial cross-section length of the sample = a

Bulged cross-section length of the sample = $R\theta$

$$\text{Strain} = \frac{\text{Change in length}}{\text{Initial length}}$$

$$\epsilon_r = \frac{R\theta - a}{a} \quad (2.3)$$

Using Taylor expansion θ can be written as:

$$\theta = \sin^{-1}(a/R) = \frac{a}{R} + \frac{(a/R)^3}{6} + \dots$$

By substituting θ in the equation (2.3), the strain (ϵ_r) in the pressurized circular sample can be expressed as:

$$\epsilon_r = \frac{a^2}{6R^2} \quad (2.4)$$

Considering the pre-existence of equi-biaxial residual stress σ_0 before pressurization the constitutive relation for the sample is

$$\sigma = \frac{E}{1 - \nu} \varepsilon + \sigma_0 \quad (2.5)$$

Noting that the stress and strain in equation (2.5) is referred to the deformed state, substituting $\sigma = \sigma_r$ and $\varepsilon = \varepsilon_r$ into the equation (2.5) the constitutive relation changes to

$$\sigma_r = \frac{E}{1 - \nu} \varepsilon_r + \sigma_0 \quad (2.6)$$

Substituting the values of σ_r and ε_r from the equation (2.2) & equation (2.4) in the equation (2.6) gives the resulting relation between the applied pressure and the radius of curvature:

$$p = \frac{E t a^2}{3(1 - \nu)} \left(\frac{1}{R} \right)^3 + 2\sigma_0 t \left(\frac{1}{R} \right) \quad (2.7)$$

where E and ν are Young's modulus and Poisson's ratio of the sample, respectively

However, the assumption of equi-biaxial stress in the circular sample^{44,48,49} leads to an underestimate in the modulus obtained from the equation (2.7). From an energy perspective, the strain energy resulting from the assumption of equi-biaxial stress σ_r and strain ε_r is $pV/3$, whereas the work done by the pressure is $pV/4$ ⁵⁰, where V is defined as the volume under the pressurized sample.

However, if a mean strain over the area of the sample is introduced as ε_m

$$\varepsilon_m = \frac{3}{4} \varepsilon_r = \frac{a^2}{8R^2} \quad (2.8)$$

The resulting strain energy is equal to the work done by the external pressure and the inconsistency between work, and strain energy is removed. This mean strain can also be derived from general elasticity⁴⁸. The validity of this mean strain measure was confirmed by Wan et al.⁴⁹,

Accordingly, equation (2.6) and equation (2.7) are changed to
Constitutive equation:

$$\sigma_r = \frac{E}{1-\nu} \varepsilon_m + \sigma_0 \quad (2.9)$$

For consistency, the pressure-radius of curvature relation becomes

$$p = \frac{Eta^2}{4(1-\nu)} (1/R)^3 + 2\sigma_0 t (1/R) \quad (2.10)$$

By substituting the value of the radius of curvature (R) in terms of central deflection (h) into the equation (2.10), a relation between the pressure and the maximum central deflection of the sample is determined as shown in the equation (2.11)

$$p = \frac{2Et}{(1-\nu)a^4} h^3 + 4\sigma_0 t \left(\frac{h}{a^2}\right) \quad (2.11)$$

2.1.2 Rectangular profile

A rectangular orifice on the substrate results in a rectangular profile on the sample subjected to the applied pressure. A schematic of the rectangular profile is shown in Figure 2.5.

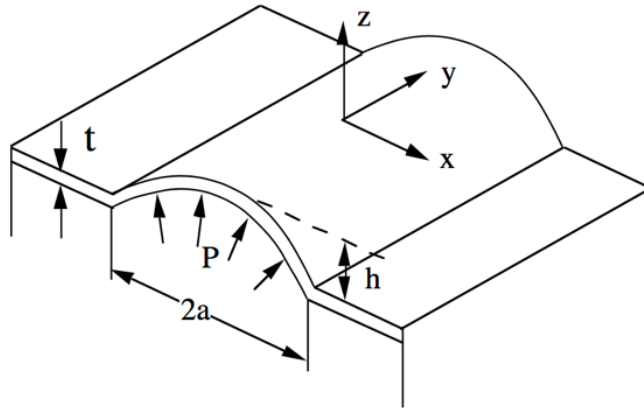


Figure 2.5: Schematic diagram of the bulged rectangular sample

The rectangular sample for bulge test should feature an aspect ratio (length/width as shown in Figure 2.6) larger than four, to reduce the shape deviation effect⁵¹.

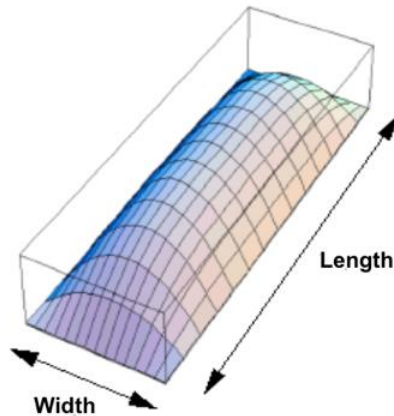


Figure 2.6: Sketch indicating aspect ratio and shape deviation effect⁵¹ of the rectangular sample

From the strain along x-direction and y-direction, it can be stated that, as long as the aspect ratio is large enough (Length/Width>4), strain in the x-direction is relatively large, while strain in the y-direction is minimal and thus can be neglected ($\epsilon_y = 0$). Furthermore, away from the ends of the rectangle, the film is assumed to have a uniform radius of curvature.

Although the stress and strain in the rectangular sample are in a state of plane stress, this is a plane-strain condition^{41,46,52,53} due to the independence of coordinate in the length/y-direction. The pressurized circular sample was modeled as a section of a thin-walled half sphere; similarly, the pressurized rectangular sample can be modeled as a thin-walled semi-cylinder, as shown in Figure 2.7.

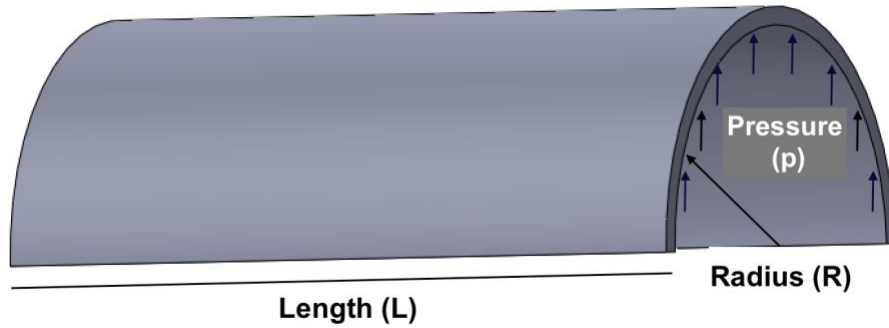


Figure 2.7: Thin-walled half cylinder model subjected to uniform pressure (p)

By force equilibrium within a semi-cylinder, the stress in the width/x-direction is calculated as:

$$\sigma_x \cdot 2t \cdot L = p \cdot 2R \cdot L$$

$$\sigma_x = \frac{pR}{t} \quad (2.12)$$

The equation (2.12) indicates the relation between the applied pressure (p), the radius of curvature (R), and stress in the bulged thin sample (σ_x).

For a pressurized rectangular sample, Figure 2.5, we can show that the cross-section bulged shape is parabolic, and the radius of curvature (R) of the bulged sample is where h is the maximum deflection, and a is the width of the sample ($h \ll a$).

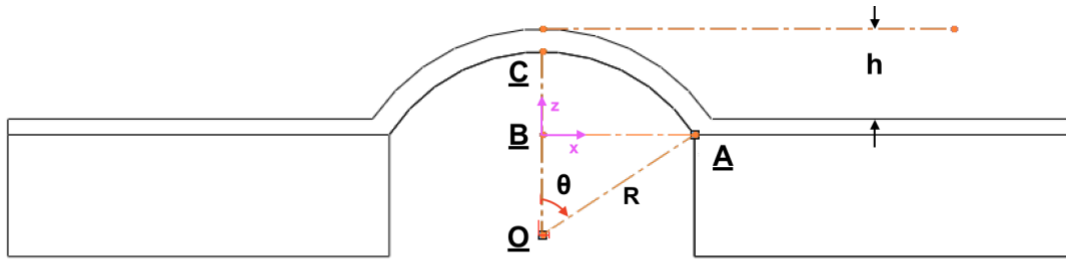


Figure 2.8: Schematic diagram showing the relation between geometric parameters of the rectangular bulge sample

From Figure 2.8, assuming the bulge deflection is symmetric along the z -axis, the geometric relation between the maximum deflection (h) and the radius of sample (a) is shown. For small deflections of the sample, the maximum central deflection is much less than the radius of the sample ($h \ll a$).

From the $\triangle OAB$ using Pythagoras theorem, a relation between maximum deflection (h), sample width (a) and radius of curvature of the rectangular sample (R) can be determined.

$$\begin{aligned}
 R^2 &= (R - h)^2 + a^2 \\
 \Rightarrow R^2 &= R^2 - 2Rh + h^2 + a^2 \\
 \Rightarrow 2Rh &= h^2 + a^2
 \end{aligned}$$

as $h \ll a$, h^2 is very small and can be neglected,

$$2Rh = a^2$$

The radius of curvature (R) of the bulged sample is

$$R = \frac{a^2}{2h} \quad (2.13)$$

The corresponding strain ε_x in the sample can be derived using the change in cross-section length of the sample before and after the bulge. From Figure 2.8,

$$\sin(\theta) = a/R$$

Initial cross-section length of the sample = a

Bulged cross-section length of the sample = $R\theta$

$$\text{Strain} = \frac{\text{Change in length}}{\text{Initial length}}$$

$$\varepsilon_x = \frac{R\theta - a}{a} \quad (2.14)$$

Using Taylor expansion θ can be written as:

$$\theta = \sin^{-1}(a/R) = \frac{a}{R} + \frac{(a/R)^3}{6} + \dots$$

Strain (ε_x) in the pressurized rectangular sample can be expressed as:

$$\varepsilon_x = \frac{a^2}{6R^2} \quad (2.15)$$

Considering the residual stresses σ_{x_0} and σ_{y_0} in the width and length directions, respectively and assuming that the strain in the length direction $\varepsilon_{y_0} = \varepsilon_y = (\sigma_{y_0} - \nu\sigma_{x_0})/E$; during pressurization, the constitutive relationship between σ_x and ε_x is written as:

$$\sigma_x = \frac{E}{1 - \nu^2} (\varepsilon_x + \varepsilon_{x_0} + \nu\varepsilon_{y_0}) \quad (2.16)$$

Where $\varepsilon_{x_0} = (\sigma_{x_0} - \nu\sigma_{y_0})/E$; is the residual strain in the width direction. By substituting the values of ε_{x_0} and ε_{y_0} , the constitutive relation changes to

$$\sigma_x = \frac{E}{1 - \nu^2} \varepsilon_x + \sigma_{x_0} \quad (2.17)$$

Substituting the values of σ_x and ε_x from the equation (2.12) & equation (2.15) in the equation (2.17) gives the resulting relation between the applied pressure and the radius of curvature:

$$p = \frac{E t a^2}{6(1 - \nu^2)} \left(\frac{1}{R}\right)^3 + \sigma_0 t \left(\frac{1}{R}\right) \quad (2.18)$$

Where E and ν are Young's modulus and Poisson's ratio of the sample respectively.

By substituting the value of the radius of curvature (R) in terms of central deflection (h) into the equation (2.18) a relation between the pressure and the maximum central deflection of the rectangular sample is determined and shown in the equation (2.19)


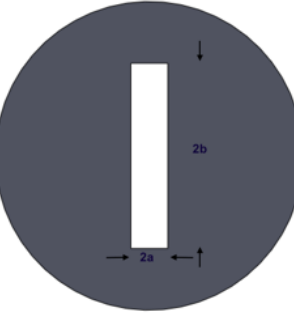
Pressure vs. max. central deflection relation (bulge equation) for the rectangular bulge test:

$$p = \frac{4Et}{3(1 - \nu^2)a^4} h^3 + 2\sigma_0 t \left(\frac{h}{a^2}\right) \quad (2.19)$$

2.1.3 Extraction of mechanical properties

Theoretical bulge equations for the circular and rectangular profiles, equations (2.11) & (2.19), along with the bulge test experiment results help extract the mechanical properties of the sample. Table 2.1 shows the summary of bulge equations for circular and rectangular samples.

Table 2.1: Summary of bulge equations for different sample geometries used in the bulge test experiment for extracting its mechanical properties

Geometry	Constitutive relation	Bulge equation
	$\sigma_r = \frac{E}{1-\nu} \varepsilon_m + \sigma_0$	$p = \frac{2Et}{(1-\nu)a^4} h^3 + 4\sigma_0 t \left(\frac{h}{a^2}\right)$ $C_1 = \frac{2Et}{(1-\nu)a^4}; C_2 = \frac{4\sigma_0 t}{a^2}$
	$\sigma_x = \frac{E}{1-\nu^2} \varepsilon_x + \sigma_{x0}$	$p = \frac{4Et}{3(1-\nu^2)a^4} h^3 + 2\sigma_0 t \left(\frac{h}{a^2}\right)$ $D_1 = \frac{4Et}{3(1-\nu^2)a^4}; D_2 = \frac{2\sigma_0 t}{a^2}$

Uniform pressure is applied to the sample (film/membrane), and the resulting central deflection is observed. The p-h response for both circular and rectangular samples are

plotted. It is seen from the equation (2.11) that the coefficient of the h^3 term from the p-h response for the circular sample is

$$C_1 = \frac{2M_c t}{a^4}, \quad (2.20)$$

where M_c is the biaxial modulus of the circular sample

$$M_c = \frac{E}{1 - \nu}. \quad (2.21)$$

Similarly, from the equation (2.19) the coefficient of the h^3 term from the p-h response for the rectangular sample is

$$D_1 = \frac{4M_r t}{3a^4}, \quad (2.22)$$

where M_r is the reduced modulus of the rectangular sample

$$M_r = \frac{E}{1 - \nu^2}. \quad (2.23)$$

The residual stresses (σ_0) & (σ_{x0}) for the circular and rectangular samples can be calculated from the linear coefficient terms (C_2) & (D_2) from the corresponding p-h responses.

Poisson's ratio can be determined by combining both equation (2.21) and equation (2.23).

$$\nu = \frac{M_c - M_r}{M_r} \quad (2.24)$$

Young's modulus (E) follows from equation (2.21) or equation (2.23)

2.2 PARAMETRIC STUDY

Schematic of the laminate, Figure 2.9, and the bulge test technique concepts were considered for the analysis of the design parameters. These design variables are listed in Table 2.2.

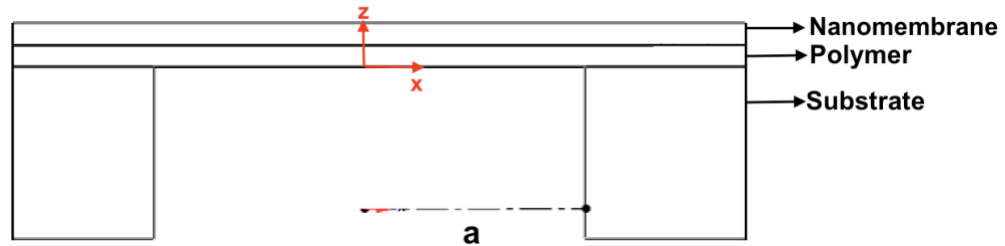


Figure 2.9: Cross-sectional schematic diagram of the composite deposited on the substrate with an orifice

Table 2.2: Bulge test design parameters

	Design parameter
1	Bulge pressure (p)
2	Polymer selection (material)
3	Polymer thickness (t_1)
4	Ge-NW membrane thickness (t_2)
5	Deflection measuring technique
6	Hole radius/ Rectangle width (a)

The bulge equation for the circular sample was considered to determine the suitable range for each parameter. The residual stress (σ_0) from the bulge equation was neglected to simplify the analysis. The simplified bulge equation is given in equation (2.25). Due to the random network of the germanium nanowires within the membrane, the lower bound on the elastic modulus of the laminate was considered as shown in equation (2.27).

$$p = \frac{2Et}{(1 - \nu)a^4} h^3. \quad (2.25)$$

In equation (2.25),

$$t = t_1 + t_2, \quad (2.26)$$

$$\frac{1}{E} = \frac{1}{E_C} = \frac{V_P}{E_P} + \frac{V_{NW}}{E_{NW}}, \quad (2.27)$$

$$\text{and } \nu = \nu_C = \nu_P * V_P + \nu_{NW} * V_{NW}, \quad (2.28)$$

where V_P = Volume fraction of the polymer
 V_{NW} = Volume fraction of germanium nanowire membrane
 E_P = Young's modulus of the polymer
 E_{NW} = Young's modulus of germanium nanowire membrane
 t_1 = Thickness of polymer film
 t_2 = Thickness of germanium nanowire membrane

The required pressure range for the bulge test experiment was determined as described in section 2.2.1. Out of the many options for polymer films, the most suitable polymer material for the experiment was determined as described in section 2.2.2. For accurately measuring the mechanical properties of germanium membrane, the best possible thickness values for both polymer film and germanium membrane were determined as defined in section 2.2.3. The range of bulge deflections determined from these sections was considered for selecting a deflection measuring technique and device.

2.2.1 Pressure selection

As mentioned in Chapter 1, a composite made of polymer and germanium nanowire membrane is tested on the setup to determine the mechanical properties of germanium nanomembrane.

We can conveniently find the mechanical properties of the existing polymer films (for example PMMA/PDMS/PET). So, an initial study was conducted just on the polymers to determine the pressure range required to create a bulge deflection that could be measured using the existing techniques.

The mechanical properties and the thickness of the polymer films generally available in the market or obtained from spin-coating are mentioned in Table 2.3

Table 2.3: Design parameter range of values for polymers (ref. CES Edu pack)

	PMMA	PDMS	PET
Young's modulus (E), MPa	500-4000	2-6	1000-5000
Poisson's ratio (ν)	0.35	0.35	0.4
thickness (t), μm	0.5-9	1-20	0.5-20

Note: For convenience, referring to Table 2.3, the design parameter values mentioned in Table 2.4 are chosen for this study.

Table 2.4: Chosen design parameter value (polymers) for the parametric analysis

	PMMA	PDMS	PET
Young's modulus (E), MPa	2000	3	2000
Poisson's ratio (ν)	0.35	0.35	0.4
thickness (t), μm	3	3	3

Various researchers have implemented the determination of the out-of-plane bulge deflection via optical microscopy with a calibrated vertical displacement⁵⁴, laser interferometry^{41,55}, position sensitive detectors (PSD) with scanning laser beams^{52,56,57} and shadow moiré⁵³. In all these techniques, the measured signals result from light beams that are reflected from the bulged film surface. Bulge deflections in the range of 100 *nm* to 100 μm can be detected using these techniques. Higher bulge deflections, such as 100 μm to several *mm*, can be measured using a digital camera or digital image correlation technique.

From the above measuring techniques, a bulge deflection (*h*) within the range of 100 μm to 1 *mm* can be conveniently measured at a low cost using a digital camera. By considering the design parameter values for polymers mentioned in Table 2.4 and the bulge deflection values (*h*) in the range of 100 μm to 1 *mm* into the equation (2.25) yields a corresponding range for the bulge pressures (*p*) as shown below.

Table 2.5: Required bulge pressure range for each polymer

	PMMA	PDMS	PET
Pressure (P), Pa	27-29500	0.045-350	27-29500

From the above analysis, a convenient deflection measuring technique and a low-cost experimental setup can be achieved when bulge pressures are in the range of 0-35kPa (0-5Psi) with 1% increments. Thus, applied bulge pressures from 0-35kPa with 0.35kPa increments are highly desired to give a measurable bulge deflection of 100 μm to 1 *mm*.

2.2.2 Polymer selection

Young's modulus (E) in the equation (2.25) refers to the composite elastic modulus. These are related to the Young's modulus and Poisson's ratio of its comprising components by equations (2.27), (2.28).

By measuring Young's modulus of the composite from the bulge test experiment, we can determine the Young's modulus of the germanium nanowire membrane from the equation (2.29).

$$E_{NW} = \frac{V_{NW} * (E_P * E_C)}{(E_P - E_C * V_P)} \quad (2.29)$$

An error in the measurement of the composite modulus from the experiment should give an equivalent error in the germanium nanowire membrane modulus (with much less deviation). The best-suited polymer out of PDMS, PMMA, and PET should be selected for the experiment to reduce the inaccuracies in determination of the germanium nanowire membrane modulus (E_{NW}).

As the Young's modulus of germanium nanowire membrane (E_{NW}) is unknown, a wide range of values from 500 Pa to 500 MPa was considered, and the respective composite modulus is calculated for all three cases (PDMS, PMMA, and PET). A 10 % error was introduced in the E_C and denoted as μ_{E_C} . Substituting the error in equation (2.27) yields a new germanium nanowire membrane modulus with a deviation from the original chosen value. The error found in the germanium nanowire membrane modulus was calculated and listed in Table 2.6 (units of the elastic modulus are given in Pa).

Table 2.6: Parametric analysis using error determination technique for polymer selection (units of the elastic modulus are given in Pa)

	Elastic Modulus (PDMS)	Elastic Modulus (Ge NW)	Elastic Modulus (Composite)	Elastic Modulus (Composite_Error)	Elastic Modulus (GE-NW_Deviation)	Error (%)
1	3.00E+06	5.00E+08	5.96E+06	6.56E+06	-3.51E+07	-107
2	3.00E+06	5.00E+07	5.66E+06	6.23E+06	-8.25E+07	-265
3	3.00E+06	5.00E+06	3.75E+06	4.13E+06	6.60E+06	32
4	3.00E+06	5.00E+05	8.57E+05	9.43E+05	5.59E+05	11.9
5	3.00E+06	5.00E+04	9.84E+04	1.08E+05	5.51E+04	10.2
6	3.00E+06	5.00E+03	9.98E+03	1.10E+04	5.50E+03	10
7	3.00E+06	5.00E+02	1.00E+03	1.10E+03	5.50E+02	10

	Elastic Modulus (PMMA PET)	Elastic Modulus (Ge NW)	Elastic Modulus (Composite)	Elastic Modulus (Composite_Error)	Elastic Modulus (GE-NW_Deviation)	Error (%)
1	2.00E+09	5.00E+08	8.00E+08	8.80E+08	5.64E+08	12.8
2	2.00E+09	5.00E+07	9.76E+07	1.07E+08	5.51E+07	10.3
3	2.00E+09	5.00E+06	9.98E+06	1.10E+07	5.50E+06	10
4	2.00E+09	5.00E+05	1.00E+06	1.10E+06	5.50E+05	10
5	2.00E+09	5.00E+04	1.00E+05	1.10E+05	5.50E+04	10
6	2.00E+09	5.00E+03	1.00E+04	1.10E+04	5.50E+03	10
7	2.00E+09	5.00E+02	1.00E+03	1.10E+03	5.50E+02	10

PMMA and PET were observed to have induced a similar error (10%) in the membrane modulus, but for PDMS the membrane modulus had a more significant deviation (~50%) when the chosen E_{NW} is above 5MPa.

PMMA and PET films can be fabricated using the spin coating technique, but PET films are also readily available in the market. Due to the ease of availability, PET film was chosen as the polymer material in the composite.

2.2.3 Thickness selection

The equations (2.27), (2.28) change to

$$\frac{1}{E_C} = \frac{V_{PET}}{E_{PET}} + \frac{V_{NW}}{E_{NW}} \quad (2.30)$$

$$\nu_C = \nu_{PET} * V_{PET} + \nu_{NW} * V_{NW} \quad (2.31)$$

The volume fraction of PET and Ge NW membrane is directly proportional to the thickness of PET (t_1) and thickness of Ge NW membrane (t_2) respectively. The composite modulus depends on the volume fraction of its constituent materials, the higher volume fraction of material results in its elastic modulus having a significant effect on the resultant composite modulus. For example, if V_{PET} is much higher than V_{NW} then the value of composite modulus (E_C) which is calculated from the bulge test experiment is much closer to the PET modulus (E_{PET}) and would lead to greater inaccuracies in deriving the germanium nanowire membrane young's modulus (E_{NW}).

Thus, the relative volume fractions of the PET and Ge NW membrane should be optimized to obtain reliable results from the analysis and experiment. As the volume fraction is directly proportional to thickness, appropriate values of t_1 and t_2 should be determined. PET films of thickness about 0.5-20 μm are available in the market. Germanium-nanowire membrane of thickness in the range of 50 nm to 6 μm can be achieved using a fabrication technique discussed in section 5.3. Considering a safety factor to the possible upper limit of Ge NW membrane, a thickness of 2 μm (t_2) was chosen for this study and the appropriate PET film thickness (t_1) was determined by performing an analysis as shown in Table 2.7 (units of the elastic modulus are given in Pa, thickness/deflection is given in μm).

Table 2.7: Parametric analysis for polymer thickness selection
(units of the elastic modulus are given in Pa)

Consider,

Bulge pressure (p) = 698.4 Pa

Hole-diameter (a) = 10 mm

Poisson's ratio (ν) = $\nu_{PET} = \nu_{NW} = 0.4$

Membrane thickness (t_2) = 2 μm

equation (2.25): $p = \frac{2Et}{(1-\nu)a^4} h^3$

equation (2.26): $t = t_1 + t_2$

equation (2.29): $\frac{1}{E_C} = \frac{\nu_{PET}}{E_{PET}} + \frac{\nu_{NW}}{E_{NW}}$

Case 1: Thickness of polymer (t_1) = 2 μm

	Elastic Modulus (PET)	Elastic Modulus (Ge NW)	Elastic Modulus (Composite)	Thickness (composite)	Bulge deflection (composite) (mm)
1	2.00E+09	5.00E+08	8.00E+08	4	0.272
2	2.00E+09	5.00E+07	9.76E+07	4	0.548
3	2.00E+09	5.00E+06	9.98E+06	4	1.173
4	2.00E+09	5.00E+05	1.00E+06	4	2.526
5	2.00E+09	5.00E+04	1.00E+05	4	5.442
6	2.00E+09	5.00E+03	1.00E+04	4	11.726
7	2.00E+09	5.00E+02	1.00E+03	4	25.263

Case 2: Thickness of polymer (t_1)= 4 μm

	Elastic Modulus (PET)	Elastic Modulus (Ge NW)	Elastic Modulus (Composite)	Thickness (composite)	Bulge deflection (composite) (mm)
1	2.00E+09	5.00E+08	1.00E+09	6	0.220
2	2.00E+09	5.00E+07	1.43E+08	6	0.422
3	2.00E+09	5.00E+06	1.49E+07	6	0.896
4	2.00E+09	5.00E+05	1.50E+06	6	1.928
5	2.00E+09	5.00E+04	1.50E+05	6	4.153
6	2.00E+09	5.00E+03	1.50E+04	6	8.948
7	2.00E+09	5.00E+02	1.50E+03	6	19.279

Case 3: Thickness of polymer (t_1)= 6 μm

	Elastic Modulus (PET)	Elastic Modulus (Ge NW)	Elastic Modulus (Composite)	Thickness (composite)	Bulge deflection (composite) (mm)
1	2.00E+09	5.00E+08	1.14E+09	8	0.191
2	2.00E+09	5.00E+07	1.86E+08	8	0.351
3	2.00E+09	5.00E+06	1.99E+07	8	0.740
4	2.00E+09	5.00E+05	2.00E+06	8	1.591
5	2.00E+09	5.00E+04	2.00E+05	8	3.428
6	2.00E+09	5.00E+03	2.00E+04	8	7.387
7	2.00E+09	5.00E+02	2.00E+03	8	15.915

Case 4: Thickness of polymer (t_1)= 18 μm

	Elastic Modulus (PET)	Elastic Modulus (Ge NW)	Elastic Modulus (Composite)	Thickness (composite)	Bulge deflection (composite) (mm)
1	2.00E+09	5.00E+08	1.54E+09	20	0.127
2	2.00E+09	5.00E+07	3.04E+08	20	0.219
3	2.00E+09	5.00E+06	3.45E+07	20	0.453
4	2.00E+09	5.00E+05	3.49E+06	20	0.973
5	2.00E+09	5.00E+04	3.50E+05	20	2.096
6	2.00E+09	5.00E+03	3.50E+04	20	4.516
7	2.00E+09	5.00E+02	3.50E+03	20	9.730

For a bulge pressure of 0.7 kPa, a different combination of volume fractions and a wide range of E_{NW} values were considered and the corresponding deflections were calculated. The higher volume fraction of PET ($V_{PET}: V_{NW} = 9:1$) had a minimum deflection of 130 μm and the lower volume fraction of PET ($V_{PET}: V_{NW} = 1:1$) had a minimum deflection of 270 μm . From section 2.2.1, bulge deflections (h) of 100 μm to 5 mm can be conveniently measured at a low cost using a digital camera.

A lower volume fraction of PET is desired to reduce the inaccuracies in the deflection measurement. PET films of thickness $t_1 = 3 \mu\text{m}$ are readily available in the market and would give ideal bulge deflections $> 240 \mu\text{m}$ when the pressure is varied from 0.05 to 5 psi. However, a PET film of $t_1 = 3 \mu\text{m}$ wrinkles too much and tears while handling, making it very difficult to deposit on the substrate. PET films of thickness $t_1 = 13 \mu\text{m}$ are available in the market and also easy for handling. So, a similar analysis as shown in Table 2.7 is conducted considering thickness $t_1 = 13 \mu\text{m}$ and listed as case 5 below.

Case 5: Thickness of polymer (t_1)= 13 μm

	Elastic Modulus (PET)	Elastic Modulus (Ge NW)	Elastic Modulus (Composite)	Thickness (composite)	Bulge deflection (composite) (mm)
1	2.00E+09	5.00E+08	1.43E+09	15	0.181
2	2.00E+09	5.00E+07	3.23E+08	15	0.298
3	2.00E+09	5.00E+06	3.69E+07	15	0.615
4	2.00E+09	5.00E+05	3.74E+06	15	1.319
5	2.00E+09	5.00E+04	3.75E+05	15	2.841
6	2.00E+09	5.00E+03	3.75E+04	15	6.121
7	2.00E+09	5.00E+02	3.75E+03	15	13.187

A PET film of thickness $t_1 = 13 \mu\text{m}$ would give bulge deflections $> 180 \mu\text{m}$ when the pressure is varied from 0.35 to 35 kPa. Deflections above $180 \mu\text{m}$ can still be measured accurately using the digital camera. Thus, even though PET film of thickness $t_1 = 3 \mu\text{m}$ is ideal, due to the difficulty in handling PET film of thickness $t_1 = 13 \mu\text{m}$ is most optimal for the bulge test experiment.

For obtaining accurate E_{NW} from the bulge test, conveniently measuring the deflections using the available techniques, and considering the feasibility to manufacture the composite using the available fabrication techniques, thickness values of $t_1 = 13 \mu\text{m}$ and $t_2 \geq 2 \mu\text{m}$ were chosen to be used in the bulge test for Germanium nanowire membrane and PET respectively.

From the above parametric study, to measure the mechanical properties of germanium nanowire membranes using the bulge test with minimal error, a low-cost set-up, and a convenient deflection measuring technique, the values shown in Table 2.8 were chosen for developing the bulge test setup.

Table 2.8: Chosen design parameter values from the parametric study

	Design parameter	Value
1	Bulge pressure (p)	0-35 kPa (1% increment)
2	Polymer selection (material)	PET film
3	Polymer thickness (t_1)	13 μm
4	Ge NW membrane thickness (t_2)	$\geq 2 \mu\text{m}$
5	Deflection measuring device	Digital camera

CHAPTER 3: EXPERIMENT

In this chapter, the bulge test experiment setup that was designed and fabricated to test the specimens, the material preparation method and the procedure for conducting the bulge test experiment are described.

The components for the experiment were selected based on the parameter values obtained from the parametric study. The design of the experiment and the description of the apparatus for the bulge test experiment is discussed in section 3.1. The composite sample for the experiment is a bi-layered material made of a polymer film and the germanium nanowire membrane. The composite was deposited on a metal substrate. This specimen (composite on the substrate) was mounted on a critical component of the apparatus, and the bulge test experiment was conducted on the composite. The manufacturing techniques used for specimen fabrication is discussed in section 3.2. The experiment procedure for determining the pressure - deflection relation of the composite is discussed in section 3.3.

3.1 APPARATUS

The pressure - deflection characteristics of the PET/Ge NW laminate is determined using the bulge test experiment apparatus to determine the mechanical properties of germanium nanowire membrane.

A fluid is used to apply uniform pressure on the sample, and an optical device is used to measure the central bulge deflection. Thus, the pressure is given as an input to the sample, and the central deflection is taken as the output.

Therefore, an input pressure system and an output deflection measurement system were designed individually and assembled. A manifold is used to mount the specimen and connect the pressure system to apply a uniform fluid pressure on the sample. The design of the manifold is described in section 3.1.1. Design of the experiment and component selection is categorized into pressurization and deflection systems and these are described in sections 3.1.2, 3.1.3 respectively.

3.1.1 Manifold

The purpose of the manifold is not only to support the specimen on top but also connecting with various components of the pressure system. The manifold manufactured for the experiment is shown in Figure 3.1.

A circular hole was machined out on the cube-shaped aluminum die block to produce a storage tank for the fluid. The cavity in the manifold produces a laminar flow of the fluid by reducing the irregularities in pressure and generating a uniform pressure along the entire sample. Three holes (numbered 1,2,3 in Figure 3.1) were drilled and tapped on the sides of the block to allow an inlet for the fluid flow, detection of fluid pressure on the sample, and a release valve to remove the air bubbles from the fluid.

A critical point of the apparatus is the mounting of the sample on its holder. The composite to be studied is deposited on the metal substrate fabricated with a circular or rectangular window in the middle, and this entire specimen is connected to the manifold using threaded screws.

A rubber O-ring is placed inside a groove on top of the manifold. When the specimen is tightly clamped to the manifold, the O-ring seals the gap around the periphery and eliminates the water leakage. Thus, it ensures to significantly reduce the leaks from the pressure applied to the sample.

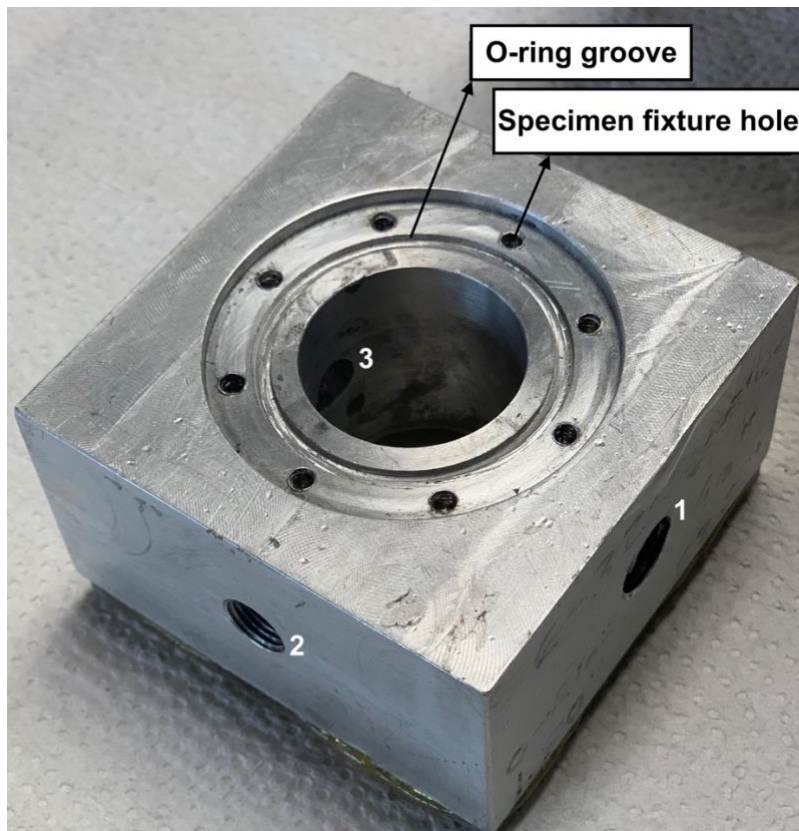


Figure 3.1: Manifold

3.1.2 Pressure System

The pressure system in the bulge test experiment should be able to store and compress the fluid, which then pressurizes the fluid within the system and applies uniform pressure on the sample. Here, the fluid pressure should not only be controlled precisely but also measured accurately.

Thus, the pressure system was categorized into two sub-systems: pressure generation and pressure detection. To accurately control and measure the pressure within the system a calibration process was done using a pressure calibration setup. The design and selection of components for pressure generation system and pressure detection system and the pressure calibration process are discussed in the following sub-sections.

Pressure Generation

From the parametric study, an input pressure from 0-35 kPa with 0.35 kPa increments is required to create a measurable bulge deflection on the composite. Water was used as the fluid in the pressure system due to its ease of availability, less density and the ability to create a uniform flow. A hydraulic syringe pump (NE500, New Era Pump Systems Inc., Wantagh, New York) compatible for generating pressures in the range of 0-70 kPa was chosen to apply pressure on the water.

The syringe pump is connected to the manifold through a 3-way aluminum valve block and a plastic tube ($\frac{1}{4}$ inch) as shown in Figure 3.2. One of the holes on the valve block is connected with a release valve which can be opened and used as a water inlet to the system.

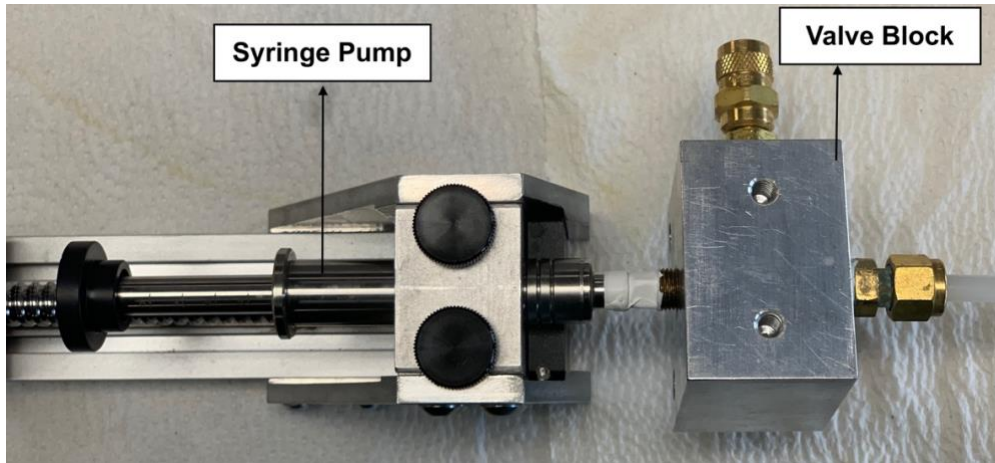


Figure 3.2: Syringe pump and valve block

The differential pressure was applied to the system by controlling the syringe pump head using a stepper motor. The stepper motor is connected to a control box, Figure 3.3, comprising Arduino board, wires, and other connections. The control box has rotating knobs to change the speed and switches to control forward/stop/reverse motion of the stepper motor. Thereby stepper motor feeds the forward, stop and reverse motion to the syringe pump head.

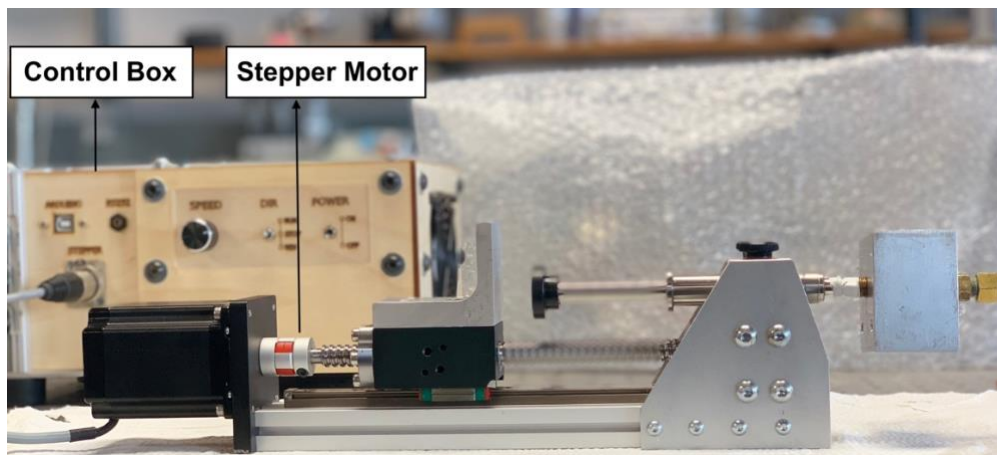


Figure 3.3: Stepper motor and control box

A schematic of the pressure generation system connecting all the components to the manifold is shown in Figure 3.4.

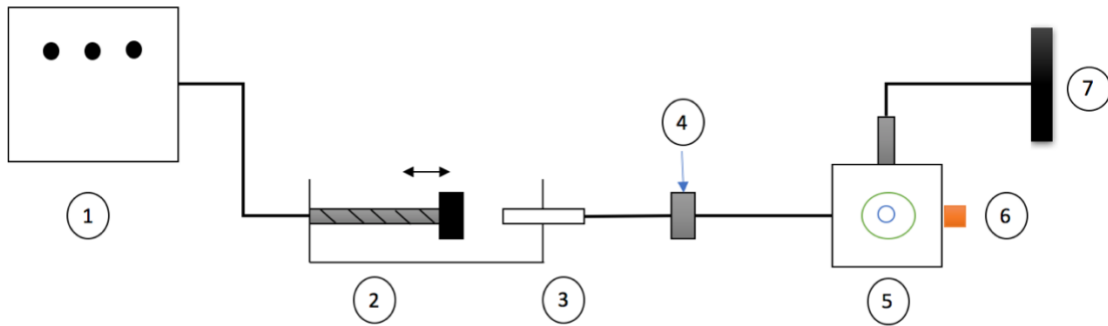


Figure 3.4: Schematic diagram of the pressure generation system

1. Motor Control box
2. Stepper Motor
3. Syringe
4. Water Inlet to valve block
5. Material over the substrate
6. Safety valve
7. Pressure detection system

Pressure Detection

A pressure transducer (Sensotec Z/0761- 09ZG, Columbus, Ohio. Capacity of 103.4 KPa) was chosen to detect the pressure within the system. The pressurized water filled in the cavity of the manifold was measured by mechanically connecting the pressure transducer to one of the holes on the manifold, shown in Figure 3.5.

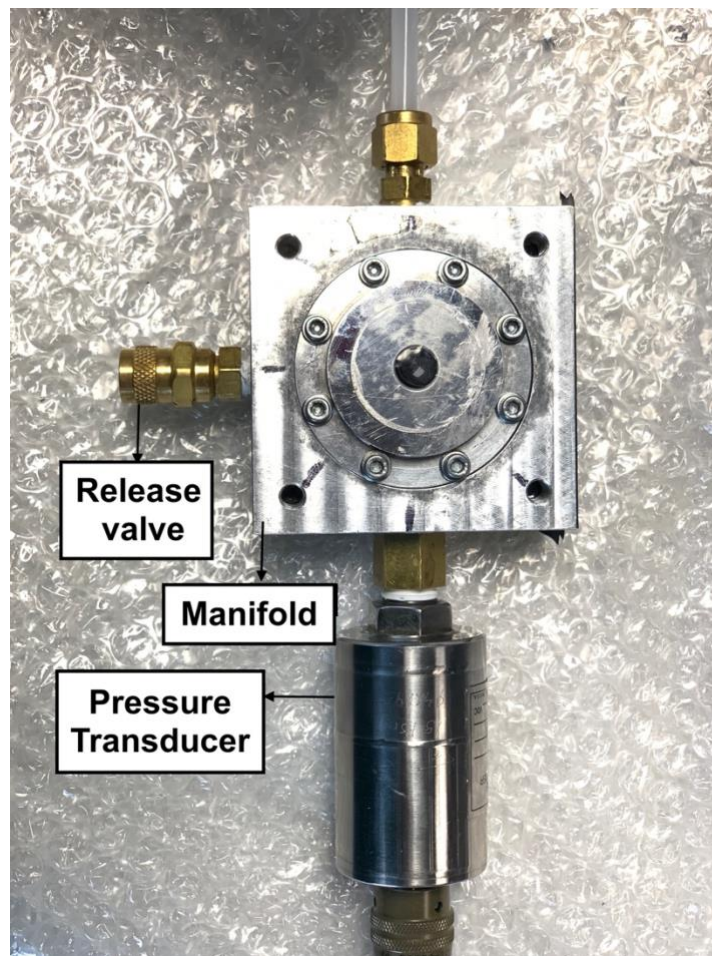


Figure 3.5: Various connections to the manifold

The pressure transducer was connected to the strain conditioner, which consists of a wheat stone bridge and an amplifier.

A voltmeter was connected to the strain conditioner, shown in Figure 3.6, to measure the change in voltage to a corresponding change in the water pressure within the system. The pressure-voltage relation was pre-determined by calibrating the pressure system setup. Thus, the value of the pressure within the system can be determined from the voltage reading on the voltmeter.



Figure 3.6: Signal conditioner and voltmeter

A schematic of the pressure detection system connecting all of its components to the manifold is shown in Figure 3.7.

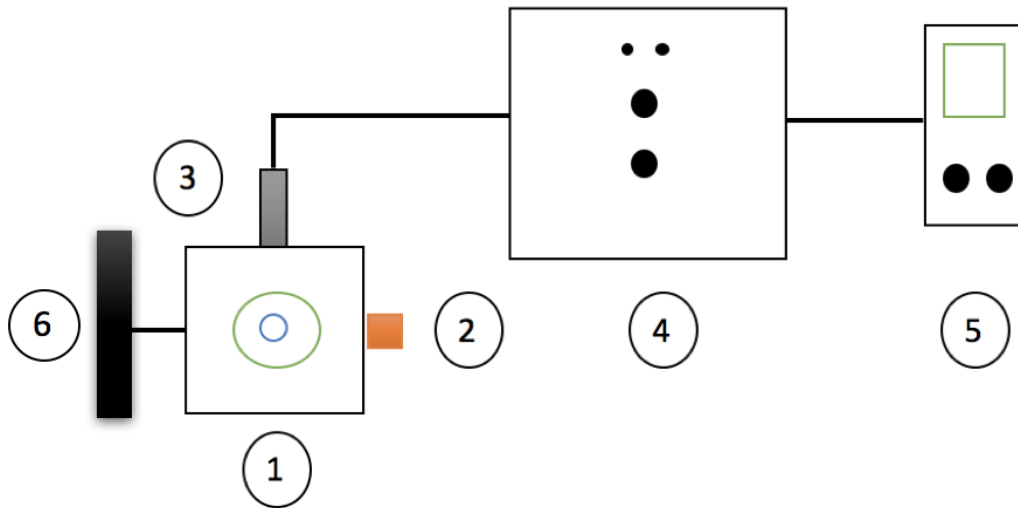


Figure 3.7: Schematic diagram of the pressure detection system

1. Material over the substrate
2. Safety valve
3. Pressure transducer
4. Signal conditioner
5. Voltmeter
6. Pressure generation system

Pressure Calibration

The pressure-voltage response for the system was calibrated, and a relation was determined to accurately measure and control pressures in the range of 0-35 kPa during the experiment.

The pressure transducer was removed from the hole and replaced with the calibration pressure transducer. The calibration pressure transducer measures the pressure (torr) and displays it on a digital meter. The electrical wiring on the calibration pressure transducer was connected to the signal conditioner.

A fully closed substrate was fabricated and connected to the manifold using threaded screws. When the system was at the initial position (syringe pump head at the top dead/fully open position), the pressure in the system was 750.8 torr (~atmospheric pressure) and the corresponding voltage value displayed on the voltmeter was set to zero by balancing and setting the gain to 20 on the signal conditioner.

The stepper motor was turned on and driven in the forward direction. The hydraulic pressure in the system was changed by 0.2 Psi increments, and the corresponding voltage values were noted down. This process was repeated for five times, and the voltage values for corresponding pressures were averaged.

The pressure vs voltage values are plotted as shown in Figure 3.8. Moreover, the relation is found to be linear. This plot can be used during the experiment to find the pressure value within the system from the voltage reading on the voltmeter.

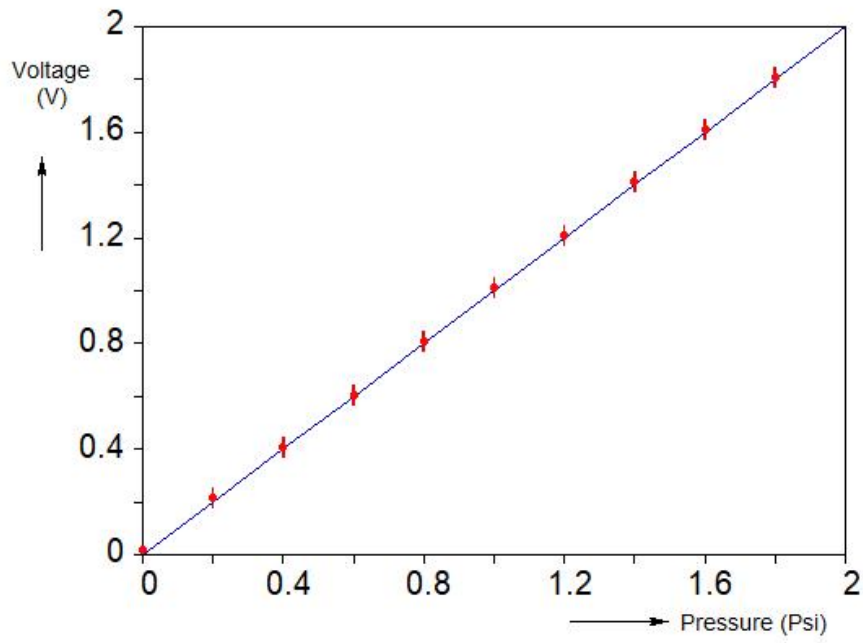


Figure 3.8: Plot showing the pressure vs voltage relation

3.1.2 Deflection system

The deflection system in the bulge test experiment should be able to measure the maximum central bulge deflection of the sample accurately. Optical measuring techniques are generally used for the bulge deflection measurement.

Components for the deflection system were chosen and modified according to the experiment requirements. To accurately measure the deflections of the sample, a deflection calibration process was accomplished using a scale. The design and selection of components for the deflection measurement system and the deflection calibration process is discussed in following sub-sections.

Deflection Measurement

From the parametric study, the bulge deflections of the composite are highly likely observed to be $\geq 100 \mu\text{m}$. Thus, a digital camera was chosen to be most convenient for the experiment. A digital camera with a 2.0x lens was placed at its focal length by the side of the manifold to measure the deflection of the bulge from the side view.

The digital camera (Lumenera corporation, Infiniti 3-3UR model, 2.8 Megapixels) was mounted on a positioner, which was placed on a mount stand as shown in Figure 3.9. This assembly controls the z-motion and gives a fine control in the x-and y-directions using the micrometers. The digital camera was connected to a computer, and the live image was viewed on the Infinity analyze software.

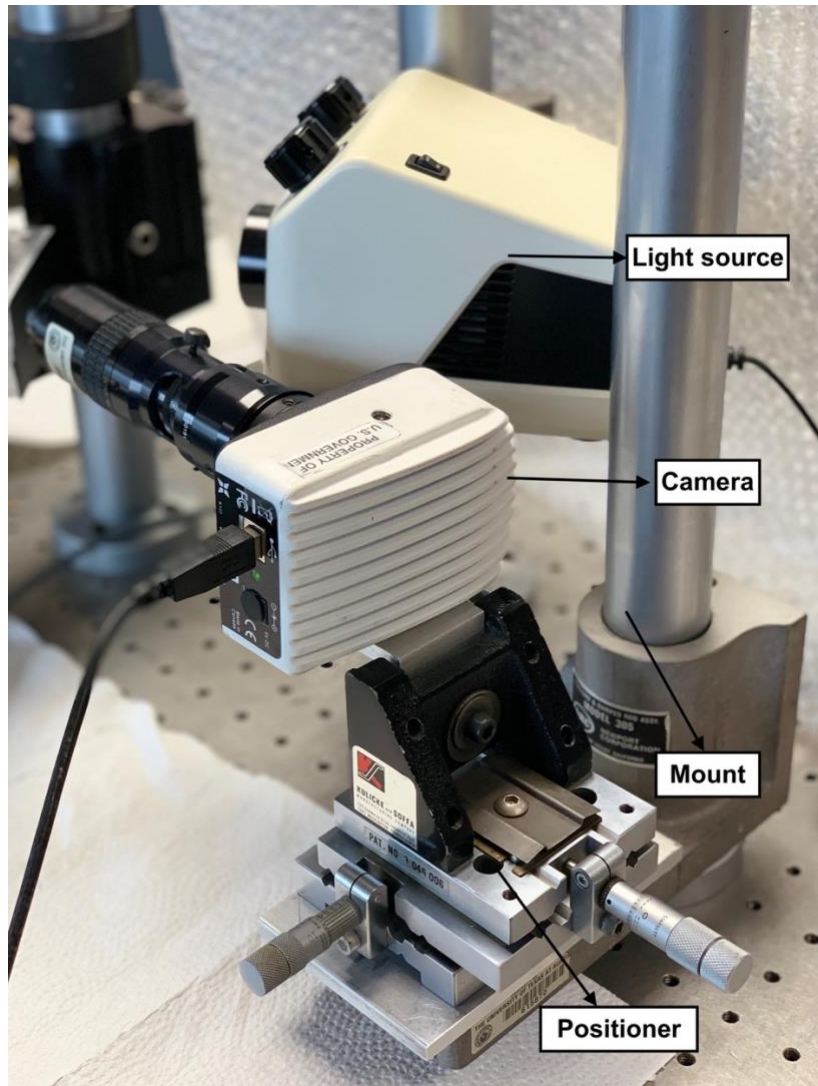


Figure 3.9: Digital camera on positioner and light source

A large mirror was mounted on a base and positioned behind the sample. A green light source placed beside the camera was directed onto the specimen. Both the mirror and the light source were used for better focus of the sample, to improve the quality of the image and to easily measure the bulge deflections.

A schematic of the deflection measurement system measuring a bulge on a sample mounted on the manifold is shown in Figure 3.10.

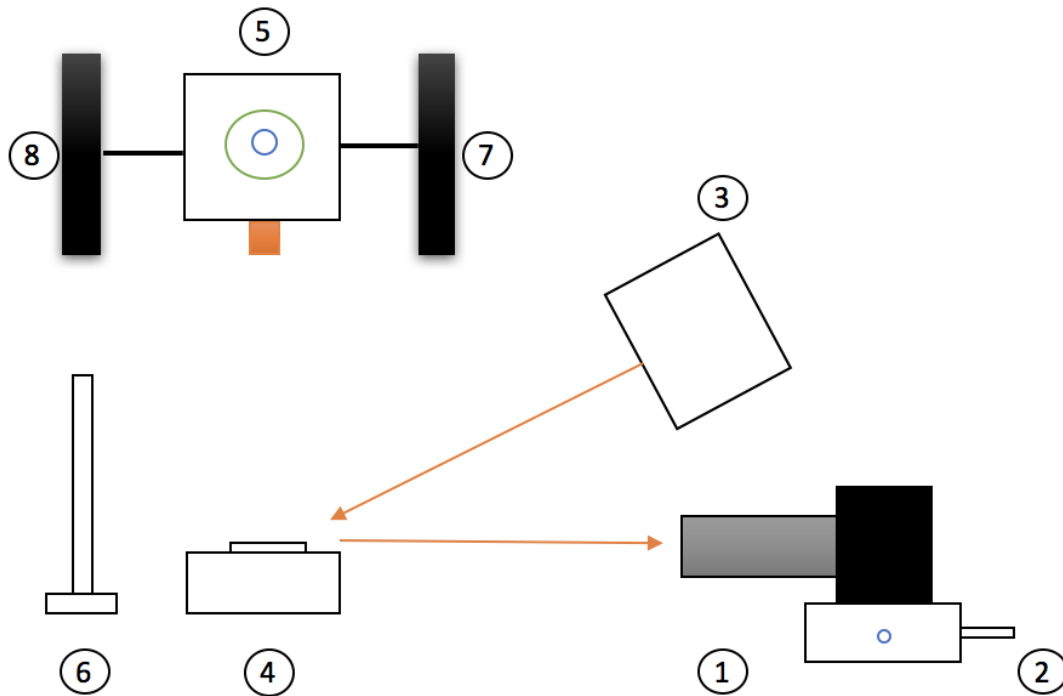


Figure 3.10: Schematic diagram of the deflection measurement system

1. Digital camera
2. Positioners
3. Light source
4. Side view of specimen on manifold
5. Top view of specimen on manifold
6. Mirror
7. Pressure generation system
8. Pressure detection system

Deflection Calibration

An area of an image is composed of numerous pixels. Each pixel represents a specific unit value. The pixel vs. unit (mm) values for the images captured on the Lumenera digital camera was calibrated, and a relation was determined to measure the bulge deflections accurately during the experiment.

A measurement paper was placed right on the substrate, and an image was captured on the infinity software. This image was opened in the ImageJ software, and under the measure section, the number of pixels between the parallel lines on the image was measured and noted down. This process was repeated for five times, and the average number of pixels between the two lines was counted and shown in Table 3.1

The distance between two lines (in pixels) = 838

The distance between the lines on the measurement paper shown in the figure was manually measured using a precise digital caliper.

Table 3.1: Pixel and length measurement values for calibration

Count	Pixels	Length (in mm)
1	838	2.49
2	841	2.50
3	837	2.49
4	838	2.50
5	839	2.50

The averaged distance between the two lines (in cm) = 2.50 mm

The averaged pixel count was equaled with the distance measured using the caliper and the relation between the pixel and unit (mm) was determined.

$$350 \text{ pixels} = 1 \text{ mm}$$

$$1 \text{ pixel} = 2.9 \text{ } \mu\text{m}$$

Using the set scale feature, the relation between pixels and mm (350 pixels/mm) was imported into the ImageJ software. This relation can be used during the experiments to measure the bulge deflection. However, the deflection calibration method should be performed before every new experiment to check the consistency of the above relation. The length/ maximum central deflection of the bulged sample was first calculated in terms of pixels and later converted to millimeters on the ImageJ software.

The pressure system and the deflection system are assembled to develop the bulge test experiment apparatus. The whole test setup is shown in Figure 3.11.

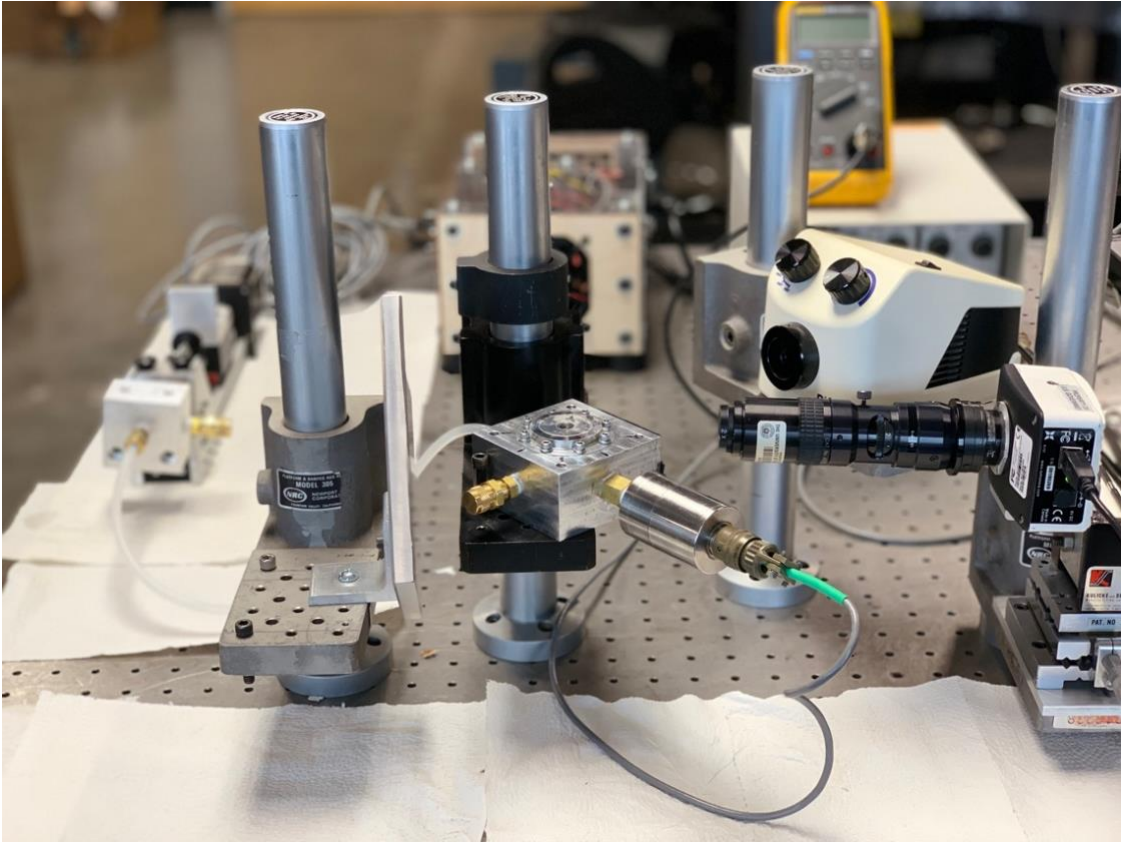


Figure 3.11: Bulge test experiment set-up

3.2 MATERIAL PREPARATION

The method used for synthesizing germanium nanowires and the polymer preparation is discussed in section 3.2.1 and 3.2.2 respectively. The deposition process of composite (germanium nanowire membrane on PET film) on the substrate to fabricate the final specimen is given in the section 3.2.3

3.2.1 Germanium Nanowire Synthesis

With the help of the Korgel group, germanium nanowires were synthesized using a supercritical fluid–liquid–solid (SFLS) nanowire growth reactor. The required materials and the synthesis procedure is described below.

Materials

The following materials were used for the synthesis:

1. Hydrogen tetrachloroaurate(III) trihydrate ($\geq 99.9\%$), purchased from Sigma-Aldrich.
2. Tetraoctylammonium bromide (98%), Sigma-Aldrich.
3. Sodium borohydride ($\geq 98.0\%$), Sigma-Aldrich.
4. Anhydrous toluene (99.8%), Sigma-Aldrich.
5. Diphenylgermane (DPG), Gelest Inc.
6. Trisilane (Si_3H_8), Voltaix.
7. Gold (Au) nanocrystals approximately 2 nm in diameter, capped with 1-dodecanethiol (Aldrich, g98%), were prepared in deionized water and toluene (Sigma-Aldrich, g99.5%), using the method developed by Brust et al. ⁵⁸.

Procedure

Ge nanowires were synthesized by an Au nanocrystal-seeded supercritical fluid–liquid–solid (SFLS) reaction in a 10mL titanium tubular reactor connected to high-performance liquid chromatography (HPLC) pump⁵⁹ as outlined in Figure 3.12.

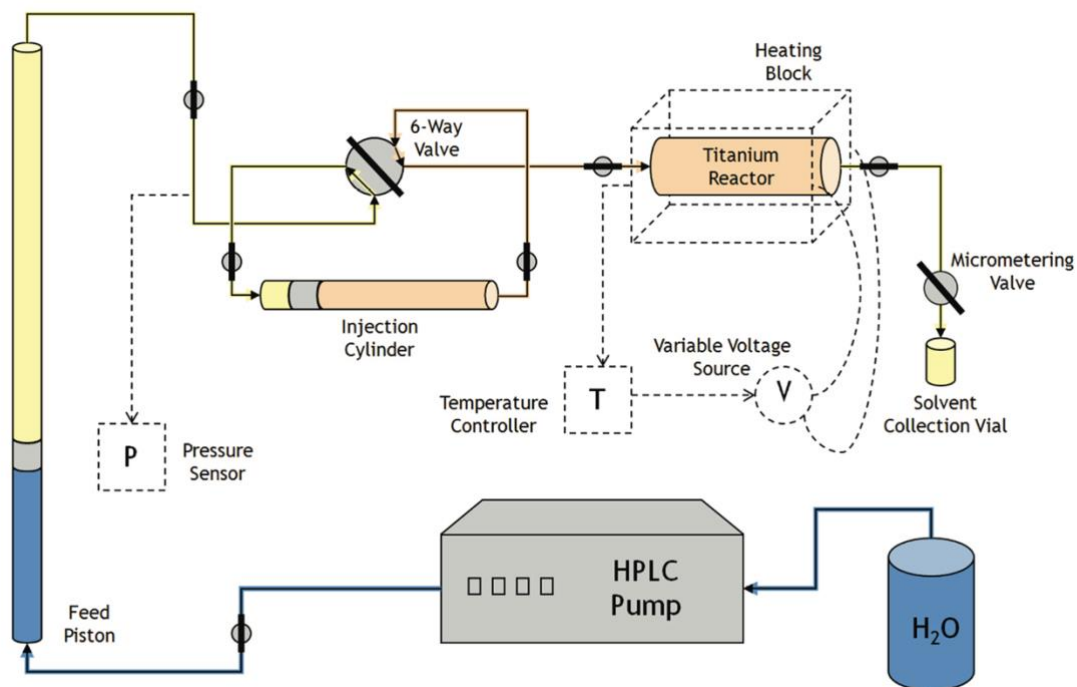


Figure 3.12: Schematic diagram of the supercritical fluid-liquid-solid (SFLS) nanowire growth reactor system

A 28 mL reactant solution of 25 μL of Au nanocrystal dispersion (20 mg/mL in toluene) and 190 μL of diphenyl germane (DPG) in anhydrous toluene was prepared in the glovebox.

Meanwhile, a 10-mL titanium tubular reactor was filled with N_2 in the glovebox and then connected to the six-way valve and the back-pressure regulator at two ends. The

reactor was preheated to 380 °C and pressurized to 10.3 MPa with anhydrous toluene using high-performance liquid chromatography (HPLC) pump

After the system had equilibrated, the solution of DPG and Au nanocrystals were injected into the reactor at a rate of 0.5 mL/min for 40 min. During this injection period, the exit stream was continually adjusted to maintain a reactor pressure of 10.3 MPa.

After completing the injection of the reactant solution, the reactor was sealed and cooled to 150 °C. An amorphous Si (a-Si) shell was then deposited on the nanowires. A volume of 42 µL of trisilane diluted in 2 mL of toluene was loaded in a syringe and injected to the reactor via the six-way valve (caution: trisilane is volatile, highly flammable and pyrophoric). Preparation of the dilute trisilane solution must be carried out inside an inert gas filled glovebox. After injection of the trisilane solution was complete, the reactor was resealed and heated to 250 °C. After 12 h, the nanowire product was purified by re-dispersion in a 2:1:1 volume mixture of chloroform, toluene, and ethanol, followed by centrifugation at 8000 rpm for 5 min. This washing procedure was repeated two more times to remove excess passivating ligand and unreacted phenyl germane. The nanowires were then dried under vacuum and stored in air under ambient conditions.

3.2.2 PET Film

A 13-micron thick Polyethylene Terephthalate film was purchased from GoodFellow corporation. The PET film was cut into circular samples of 30 mm diameter using a laser cutting machine (LPKF protolaser), shown in Figure 3.13. Laser cutting method not only improves the accuracy of the shape of the film but also reduces the wrinkles developed in the film.

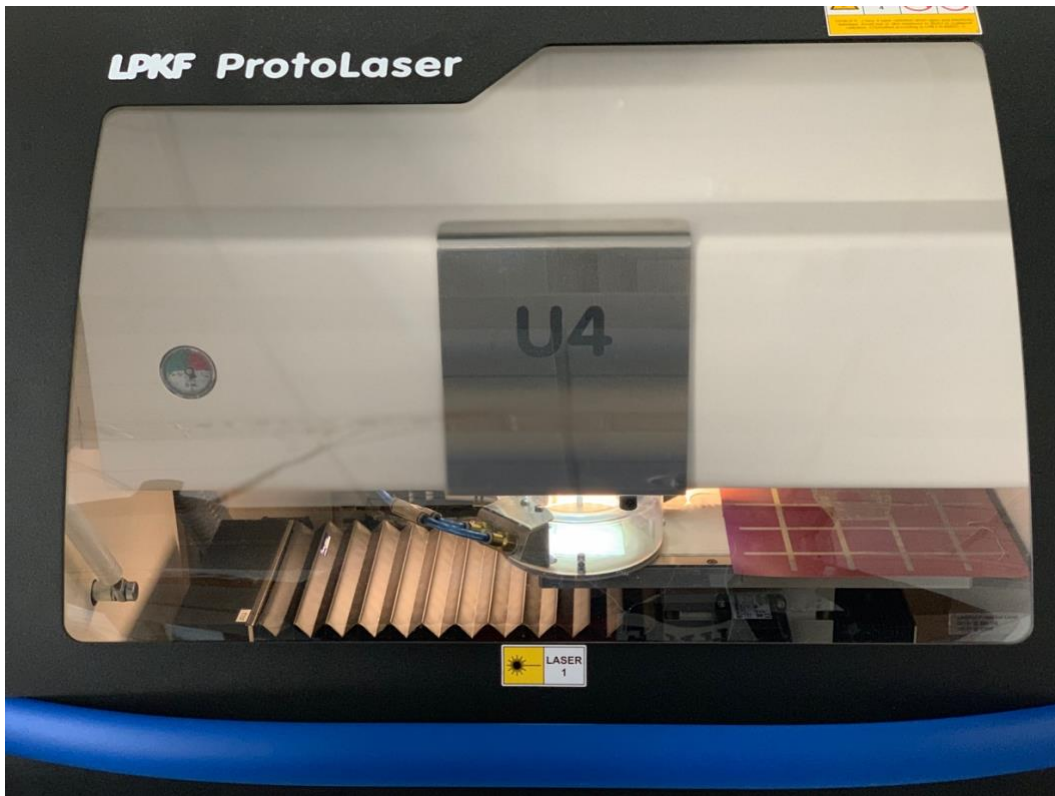


Figure 3.13: LPKF Protolaser cutting machine

The PET film was placed on a rubber mat inside the chamber of the laser cutter. PET film was stretched and wholly pressed onto the rubber mat when the vacuum underneath the mat was turned ON. A circular profile drawing was designed in the LPKF circuit pro software connected to the laser cutter. The number of passes and power of the laser was assigned as 25 and 5 W respectively in the LPKF circuit pro settings. The laser cutting process was executed, and the circular PET film samples of 30mm diameter were fabricated as shown in Figure 3.14.

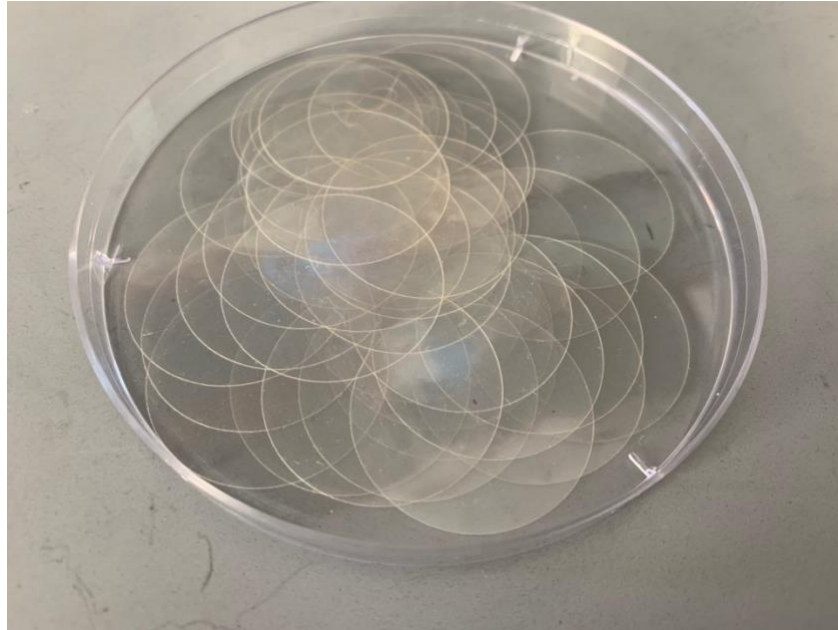


Figure 3.14: Circular PET samples cut (OD-30 mm)

3.2.3 Specimen

Multiple aluminum and copper substrates were fabricated to facilitate the deposition of the composite (PET and Ge-NW membrane). Aluminum blocks were machined into thin cylindrical pieces. A circular hole of 10mm diameter was cut at the center of each piece. A machine lathe was used to taper the hole outward with an angle of 25 degrees onto the bottom side. This helps reduce air pockets forming during filling. The PET film was attached to the substrate using a 3M double coated medical tape (transparent polyethylene tape, 80 microns).

For the circular bulge test, the medical tape was cut into a concentric circular shape of 10 mm inner diameter and 30 mm outer diameter with the laser cutting machine, using a similar process described in section 3.2.2. The concentric circular medical tape sample is shown in Figure 3.15.

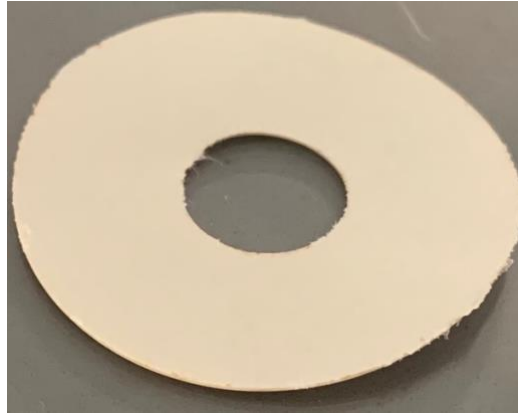


Figure 3.15: Concentric circular double-sided tape (OD-30mm, ID- 10mm)

First, the carrier on one side of the medical tape was removed using a tweezer. The adhesive side of the tape was placed on the substrate such that the inner concentric hole of the tape aligns with the 10mm circular hole on the substrate. Next, the carrier on the other side of the tape was removed, and the circular PET film of 30 mm diameter was placed right on top of the open adhesive side of the tape, such that the PET film completely aligns with the outer edges of the tape. With this process, a freestanding circular PET film on the substrate was fabricated. The PET film on the substrate is shown in Figure 3.16.



Figure 3.16: PET film attached to the substrate with circular orifice

For the rectangular bulge test, the medical tape was cut into a 30mm diameter circle with a concentric rectangular shape of 20 mm length and 4 mm width with the laser cutting machine, using a similar process shown in the section 3.2.2. The concentric rectangular medical tape sample is shown in Figure 3.17.

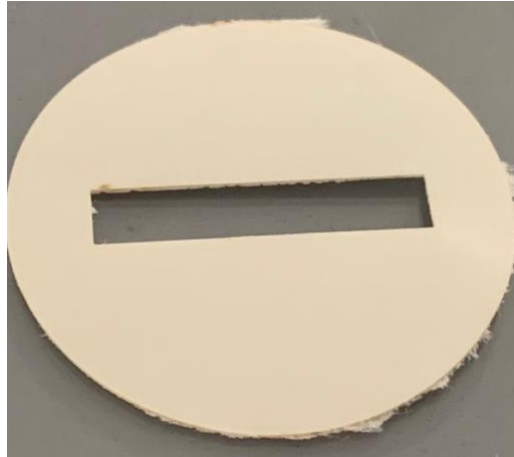


Figure 3.17: Concentric rectangular double-sided tape (OD-30mm, ID- 20mm*4mm)

Similarly, the carrier on one side of the medical tape was removed using a tweezer. The adhesive end of the tape was placed on the substrate such that the inner concentric rectangle of the tape aligns with the 20mm length and 4 mm width dimensions on the substrate. Next, the carrier on the other side of the tape was removed, and the PET film of 30 mm diameter was placed right on top of the open adhesive side of the tape, such that the PET film completely aligns with the outer edges of the tape. With this process, a freestanding rectangular PET film on the substrate was fabricated. The PET film on the substrate is shown in Figure 3.18.

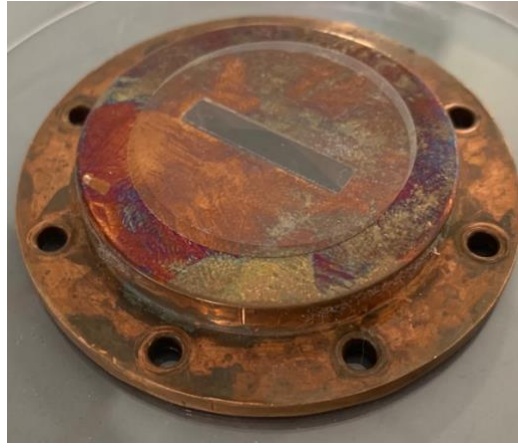


Figure 3.18: PET film attached to the substrate with rectangular orifice

The germanium nanowires developed by the Korgel group are treated and loaded into the spray coater, Figure 3.19.



Figure 3.19: Spray coating machine



Figure 3.20: Composite (Ge-NW membrane deposited on PET) on the substrate:

The PET film on the substrate was kept inside the spray coating chamber, 6 mg of germanium nanowires were sprayed by running across the sample. Thickness of the sample was measured under scanning electron microscopy; SEM image is shown in Figure 3.21. A germanium nanowire membrane of $5 \pm 0.3 \mu\text{m}$ thick was formed on top of the PET film as shown in Figure 3.20.

Thus, the composite made of the polymer film and germanium nanowire membrane was deposited on the substrate (copper/aluminum) by using a double-sided medical tape and spray coater respectively. The final specimen was further used for testing on the bulge test apparatus.

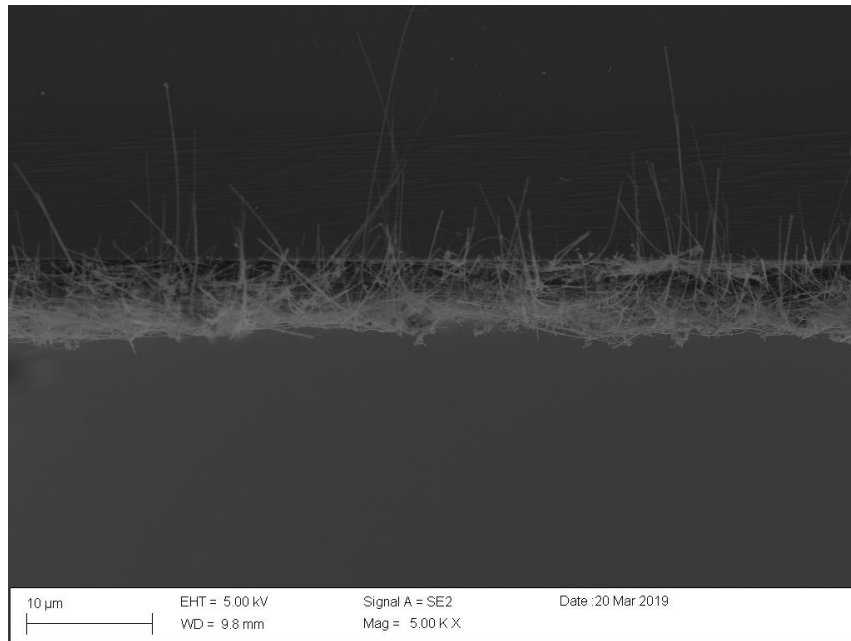


Figure 3.21: SEM image of the spray coated sample

3.3 EXPERIMENT PROCEDURE

A step by step procedure for conducting bulge test experiment to determine the pressure-deflection relation of the composite is shown below:

1. The vacuum grease is applied to the O-ring of the manifold, and the fabricated specimen (composite deposited on the aluminum substrate) is mechanically fixed to the manifold using screws.
2. The water is filled into the system through a hole opened by removing the release valve on the 3-way aluminum valve block.
3. While filling the water, the release valve on the manifold is slightly turned to remove the air entrapped within the system. This process ensures the removal of water bubbles completely and reduces the error in the measured pressure.
4. Once the water is completely filled, the release valve is connected to the 3-way aluminum valve block.
5. The light source on the specimen is turned ON, and the Infinity analyze software is opened on the computer. A calibration paper is placed across the diameter of the specimen, and the camera is aligned perfectly with the composite by adjusting the x, y and z directions on the camera mount.
6. The voltmeter is set to zero volts by adjusting the balance knob on the signal conditioner; it corresponds to a bulge pressure of 0 kPa.
7. The stepper motor is turned ON, and a very low rpm is chosen using the knobs on the control box.
8. The stepper motor is turned off after every 0.35 kPa increment in pressure, and the bulge deflection image is captured on the infinity analyze software. This process is continued until the system reaches a pressure of 7 kPa.
9. Using ImageJ software, the maximum central deflection of the bulge on each image is measured and tabulated along with their corresponding bulge pressure values.

CHAPTER 4: RESULTS

Both circular and rectangular composite samples were tested on the bulge test apparatus. The mechanical properties of the composite were determined from the bulge test and subsequently the elastic material properties of the germanium nanowire membrane were extracted. Results from the bulge test experiment are presented in this chapter.

DATA ANALYSIS

Pressure and the maximum central deflection measurements obtained from the bulge test are plotted against each other. The pressure vs. deflection curve is then fitted with the bulge equation derived in chapter 2, equation (2.11) and equation (2.19) for circular sample and rectangular sample respectively. The coefficients (C_1, C_2, D_1 & D_2) determined from the curve fit are used to calculate the reduced modulus and residual stress as mentioned in section 2.1.3.

An initial bulge test was conducted on a 13 μm PET film to verify and validate the elastic properties obtained from the experiment result with the known values. Five repetitions of bulge test on the PET film were conducted and the coefficients obtained from the curve fit, Figure 4.1, along with the equations (2.11) and (2.19) were used to determine the elastic properties. Young's modulus and Poisson's ratio obtained from the bulge test experiment were 2.55 ± 0.12 GPa & 0.393 ± 0.015 , respectively. This result is consistent with the known $E = 2.5$ GPa and $\nu = 0.4$ for the 13micron PET film (GoodFellow corporation) with an error of 2 %.

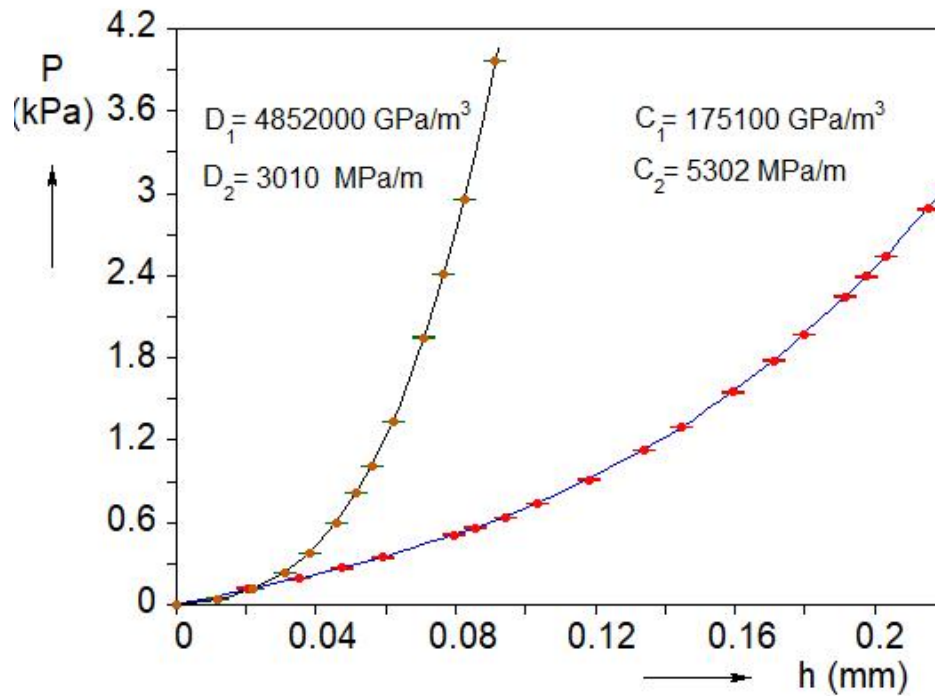


Figure 4.1: Pressure vs deflection plot for the 13micron PET film from the bulge test

The bulge test experiment as mentioned in section 3.3 was conducted on both circular and rectangular composite samples with five repetitions each. The average values from the test are considered to plot the pressure vs deflection curve for the circular sample, shown in Figure 4.2, and the rectangular sample, shown in Figure 4.3. The cubic and linear coefficients for both circular and rectangular samples can be determined from the curve fit with bulge equations equation (2.11) and equation (2.19) respectively.

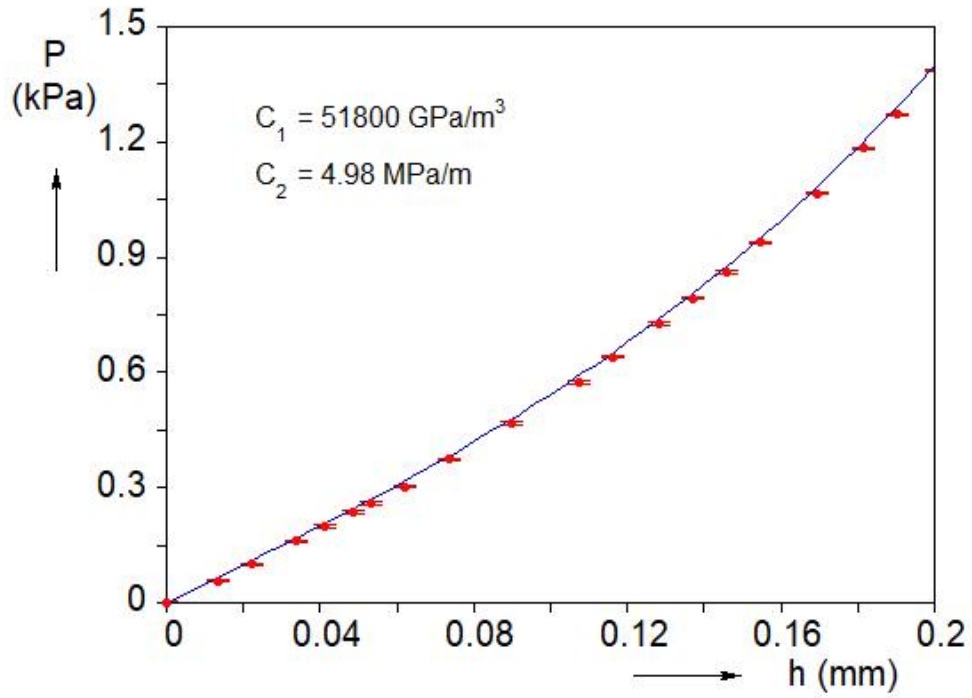


Figure 4.2: Pressure vs deflection plot for the 18micron circular composite sample from the bulge test

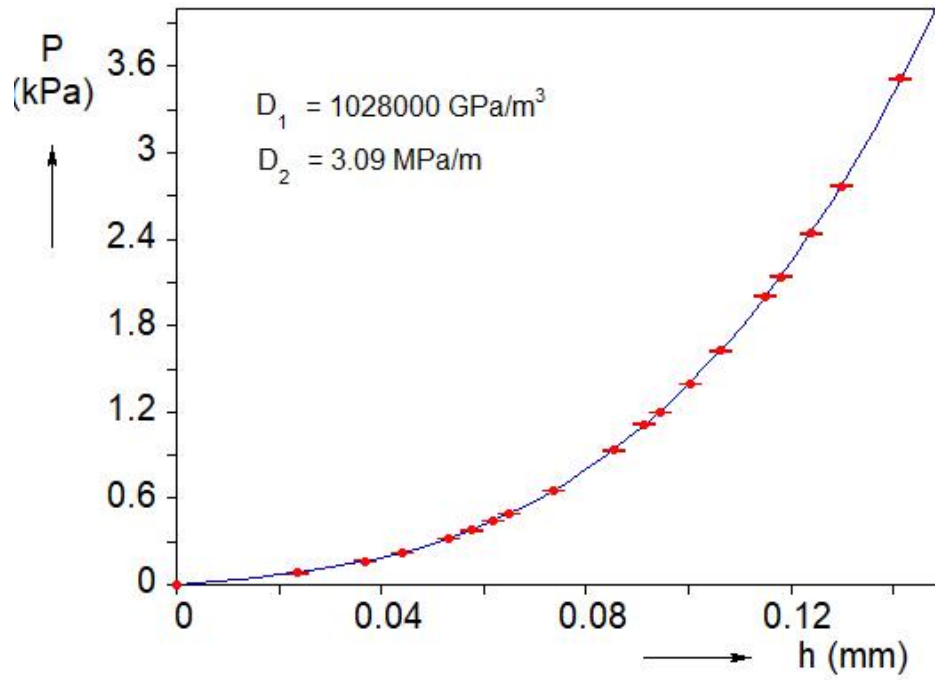


Figure 4.3: Pressure vs deflection plot for the 18micron rectangular composite sample from the bulge test

Hole-diameter (a) = 10 mm

Rectangle-width (a) = 2 mm

PET thickness (t_1) = 13 μm

Nanowire membrane thickness on the circular composite sample (t_2) = $5 \pm 0.3 \mu\text{m}$

Nanowire membrane thickness on the rectangular composite sample (t_2) = $5 \pm 0.3 \mu\text{m}$

Young's Modulus (E_{PET}) = 2.55 GPa

Poisson's ratio (ν_{PET}) = 0.393

Coefficients (C_1, C_2, D_1 & D_2) are determined from the curve fit of Figures (4.2), (4.3).

The reduced modulus (M_c) and the residual stress (σ_0) for the circular sample are:

$$M_c = 899.30 \pm 5.20 \text{ MPa}$$

$$\sigma_0 = 1.72 \pm 0.03 \text{ MPa}$$

The reduced modulus (M_r) and the residual stress (σ_{x0}) for the rectangular sample are:

$$M_r = 685.33 \pm 2.08 \text{ MPa}$$

$$\sigma_{x0} = 0.62 \pm 0.02 \text{ MPa}$$

The Poisson's ratio and Young's modulus of the composite are calculated using equations (2.21), (2.24).

$$E_c = 618.53 \pm 3.7 \text{ MPa}$$

$$\nu_c = 0.312 \pm 0.008$$

Elastic material properties of the nanowire membrane can be extracted from the following equations:

$$\frac{1}{E_C} = \frac{V_{PET}}{E_{PET}} + \frac{V_{NW}}{E_{NW}} \quad (4.1)$$

$$\nu_C = \nu_{PET} * V_{PET} + \nu_{NW} * V_{NW} \quad (4.2)$$

$$V_{PET} = \frac{t_1}{t_1 + t_2} ; V_{NW} = \frac{t_2}{t_1 + t_2} \quad (4.3)$$

Young's modulus and Poisson's ratio of the germanium nanowire membrane are:

$$\mathbf{E_{NW} = 208.30 \pm 5.2 \text{ MPa}}$$

$$\mathbf{\nu_{NW} = 0.104 \pm 0.03}$$

CHAPTER 5: CONCLUSION

Young's modulus and Poisson's ratio of the germanium nanowire membrane determined from the bulge test experiment are 208.30 ± 5.2 MPa and 0.104 ± 0.03 respectively. The values obtained from the five repetitions of the bulge test on circular and rectangular samples gave elastic properties within the range given above. An error of ± 2.5 % and ± 2.88 % was observed in Young's modulus and Poisson's ratio respectively.

This error can be due to the limitations on the deflection, pressure and the thickness measurements. The resolution of the image on the digital camera with one pixel is equivalent to $3 \mu\text{m}$. The resolution of the pressure transducer is 7 Pa which is equivalent to 0.2 % of the maximum pressure applied on the sample. The thickness of the spray coated nanowire membrane measured on the SEM was $5 \pm 0.3 \mu\text{m}$. Due to the inability to measure the change in deflection less than $3 \mu\text{m}$ and pressure less than 0.007 kPa, and the 6 % variation of the membrane thickness from spray coating could have introduced this error.

Due to the presence of visco-elastic behavior of the polymer film, the composite was allowed to rest for 24 hours before each repetition of the bulge test. It was also observed that the residual stress in the composite for both circular and rectangular samples was reduced from 1.75 MPa to 1.69 MPa and 0.64 MPa to 0.60 MPa respectively. This behavior can be attributed to the stress relaxation of the composite.

The bulge test method presented in this work is not only limited to the germanium nanowire membrane but it can also be used for determining the mechanical properties of any porous film, membrane and three-dimensional nanostructure. For example: nanocrystal films, carbon nanotube membrane etc. These materials can be deposited on a free-standing base material (either polymer or metal film) to fabricate a composite specimen. The most optimal base material can be selected by performing a parametric analysis on the composite specimen using the bulge equations.

This composite specimen can be subjected to a differential pressure by controlling the fluid volume in the bulge test apparatus. The corresponding pressure and deflection values can be measured and the pressure vs deflection characteristics of the composite can be studied to extract the mechanical properties of the material.

FURTHER WORK

An alternative approach of measuring the radius of curvature of the bulged film and converting it to the bulge deflection by equation (2.1) can be used to reduce the error in deflection measurement by the digital camera. Moire deflectometry technique is extensively used for measuring the radius of curvature of the bulged thin films. The yield behavior and other mechanical properties such as failure strength of the germanium nanowire membrane can be determined by loading the sample on the bulge test apparatus until it bursts.

To study the mechanical behavior of the nanowire membrane a two dimensional-long fiber network model of the germanium nanowire membrane is developed by the Huang group. A single layer of nanowire membrane of thickness equivalent to the diameter of the nanowire ($d = 50$ nm) was considered for the model. Mechanical properties such as

stiffness and poisson's ratio of the membrane were determined from the model. To verify and validate this model, a bulge test experiment on the 2D nanowire membrane is highly desired.

The elastic mechanical properties presented in this work were obtained from testing the 5 μm thick germanium nanowire membrane, which is equivalent to 100 layers of nanowires stacked on top of each other. Extracting the elastic material properties of a 50-nm thick germanium nanowire membrane deposited on a 13 μm thick PET on the bulge test apparatus would give higher error due to very low volume fraction of the membrane within the composite. Also, a PET film of thickness $\leq 3 \mu\text{m}$ wrinkles too much and tears while handling making it very difficult to deposit on the substrate.

Thus, due to the limitations on the thickness of the polymer an alternative method to determine the properties of the 2D nanowire membrane should be developed. One such method is to determine the elastic properties of multiple composite samples with decreasing thickness of nanowire membrane (maintaining polymer thickness constant) and extrapolating this data/trend to estimate the elastic properties of the 2D germanium nanowire membrane of 50-nm thickness.

References

- (1) Gudiksen, M. S.; Wang, J. F.; Lieber, C. M. Size-Dependent Photoluminescence from Single Indium Phosphide Nanowires. *J. Phys. Chem. B* 2002, 106, 4036–4039.
- (2) Yu, H.; Li, J. B.; Loomis, R. A.; Wang, L. W.; Buhro, W. E. Two-versus Three-Dimensional Quantum Confinement in Indium Phosphide Wires and Dots. *Nat. Mater.* 2003, 2, 517–520.
- (3) Kan, S.; Mokari, T.; Rothenberg, E.; Banin, U. Synthesis and Size-Dependent Properties of Zinc-Blende Semiconductor Quantum Rods. *Nat. Mater.* 2003, 2, 155–158.
- (4) Sun, J.; Wang, L. W.; Buhro, W. E. Synthesis of Cadmium Telluride Quantum Wires and the Similarity of their Effective Band Gaps to Those of Equidiameter Cadmium Telluride Quantum Dots. *J. Am. Chem. Soc.* 2008, 130, 7997–8005.
- (5) Wang, F.; Yu, H.; Jeong, S.; Pietryga, J. M.; Hollingsworth, J. A.; Gibbons, P. C.; Buhro, W. E. The Scaling of the Effective Band Gaps in Indium Arsenide Quantum Dots and Wires. *ACS Nano* 2008, 2, 1903–1913.
- (6) Wang, J.; Gudiksen, M. S.; Duan, X.; Cui, Y.; Lieber, C. M. Highly Polarized Photoluminescence and Photodetection from Single Indium Phosphide Nanowires. *Science* 2001, 293, 1455–1457.
- (7) Yu, Y.; Protasenko, V.; Jena, D.; Xing, H.; Kuno, M. Photocurrent Polarization Anisotropy of Randomly Oriented Nano-wire Networks. *Nano Lett.* 2008, 8, 1352–1357.
- (8) Sercel, P. C.; Vahala, K. J. Polarization Dependence of Optical Absorption and Emission in Quantum Wires. *Phys. Rev. B: Condens. Matter Mater. Phys.* 1991, 44, 5681–5691.
- (9) Hu, J.; Li, L.-s.; Yang, W.; Manna, L.; Wang, L.-w.; Alivisatos, A. P. Linearly Polarized Emission from Colloidal Semiconductor Quantum Rods. *Science* 2001, 292, 2060–2063.
- (10) Giblin, J.; Kuno, M. Nanostructure Absorption: A Comparative Study of Nanowire and Colloidal Quantum Dot Absorption Cross Sections. *J. Phys. Chem. Lett.* 2010, 1, 3340–3348.
- (11) Giblin, J.; Syed, M.; Banning, M. T.; Kuno, M.; Hartland, G. Experimental Determination of Single CdSe Nanowire Absorption Cross Sections through Photothermal Imaging. *ACS Nano* 2010, 4, 358–364.

- (12) Protasenko, V.; Bacinello, D.; Kuno, M. Experimental determination of the absorption cross-section and molar extinction coefficient of CdSe and CdTe nanowires. *J. Phys. Chem. B* 2006, 110, 25322–25331.
- (13) Hang, Q.; Wang, F.; Buhro, W. E.; Janes, D. B. Ambipolar Conduction in Transistors Using Solution Grown InAs Nanowires with Cd Doping. *Appl. Phys. Lett.* 2007, 90, 062108.
- (14) Hang, Q.; Wang, F.; Carpenter, P. D.; Zemlyanov, D.; Zakharov, D.; Stach, E. A.; Buhro, W. E.; Janes, D. B. Role of Molecular Surface Passivation in Electrical Transport Properties of InAs Nanowires. *Nano Lett.* 2008, 8, 49–55.
- (15) Protasenko, V. V.; Hull, K. L.; Kuno, M. Disorder-Induced Optical Heterogeneity in Single CdSe Nanowires. *Adv. Mater.* 2005, 17, 2942–2949.
- (16) Schaefer, S.; Wang, Z.; Kipp, T.; Mews, A. Fluorescence Modulation of Single CdSe Nanowires by Charge Injection through the Tip of an Atomic-Force Microscope. *Phys. Rev. Lett.* 2011, 107, 137403.
- (17) Vietmeyer, F.; McDonald, M. P.; Kuno, M. Single Nanowire Microscopy and Spectroscopy. *J. Phys. Chem. C* 2012, 116, 12379–12396.
- (18) Vietmeyer, F.; Tchelidze, T.; Tsou, V.; Janko, B.; Kuno, M. Electric Field-Induced Emission Enhancement and Modulation in Individual CdSe Nanowires. *ACS Nano* 2012, 6, 9133–9140.
- (19) Hanrath, T.; Korgel, B. A. Influence of Surface States on Electron Transport through Intrinsic Ge Nanowires. *J. Phys. Chem. B* 2005, 109, 5518–5524.
- (20) Schricker, A. D.; Joshi, S. V.; Hanrath, T.; Banerjee, S. K.; Korgel, B. A. Temperature Dependence of the Field Effect Mobility of Solution-Grown Germanium Nanowires. *J. Phys. Chem. B* 2006, 110, 6816–6823.
- (21) Chan, C. K.; Peng, H. L.; Liu, G.; McIlwrath, K.; Zhang, X. F.; Huggins, R. A.; Cui, Y. High-Performance Lithium Battery Anodes Using Silicon Nanowires. *Nat. Nanotechnol.* 2008, 3, 31–35.
- (22) Chan, C. K.; Zhang, X. F.; Cui, Y. High Capacity Li Ion Battery Anodes using Ge Nanowires. *Nano Lett.* 2008, 8, 307–309.
- (23) Cui, Y.; Lieber, C. M. Functional Nanoscale Electronic Devices Assembled Using Silicon Nanowire Building Blocks. *Science* 2001, 291, 851–853.
- (24) Gudixsen, M. S.; Lauhon, L. J.; Wang, J.; Smith, D. C.; Lieber, C. M. Growth of Nanowire Superlattice Structures for Nanoscale Photonics and Electronics. *Nature* 2002, 415, 617–620.
- (25) Poizot, P.; Laruelle, S.; Grugéon, S.; Dupont, L.; Tarascon, J.-M. Nano-Sized Transition-Metaloxides as Negative-Electrode Materials for Lithium-Ion Batteries. *Nature* 2000, 407, 496–499.

- (26) Law, M.; Sirbuly, D. J.; Johnson, J. C.; Goldberger, J.; Saykally, R. J.; Yang, P. Nanoribbon Waveguides for Subwavelength Photonics Integration. *Science* 2004, 305, 1269–1273.
- (27) Damon A. S.; Vincent C. H.; and Brian A. K. Flexible Germanium Nanowires: Ideal Strength, Room Temperature Plasticity, and Bendable Semiconductor Fabric, *ACS Nano*. 2010,4 (4), 2356-2362.
- (28) Kraft, O. Thin films: mechanical testing. *Encyclopedia of Materials: science and technology*. 2001, 9257-9261.
- (29) Vinci R.P; Vlassak J.J. Mechanical behavior of thin films. *Ann. Rev. Mater. Sci* 1996 ,26, 431.
- (30) Arzt E. Size effects in materials due to microstructural and dimensional constraints: A comparative review. *Acta Mater* 1998, 46, 5611.
- (31) Venkatraman R.; Bravman J.C. Separation of film thickness and grain-boundary strengthening effects in Al thin-films on Si. *J. Mater. Res* 1992, 7, 2040
- (32) Freund L.B; Suresh S. *Thin Film Materials: Stress, Defect Formation, and Surface Evolution*. Cambridge University Press 2003, 6
- (33) Nix, W.D Mechanical properties of thin films *Metall. Trans* 20A 1989, 2217-2245
- (34) Baker S.P. Nano indentation techniques. *Encyclopedia of Materials: science and technology* 2001, 5908-5915.
- (35) Read D.T.; Dally J.W. A new method for measuring strength and ductility of thin films *J. Mater* 1993, 8. 1542-1549.
- (36) Brotzen F.R. Mechanical testing of thin films. *Int. Mater* 1994, 39, 24-45
- (37) Beams J.W. Mechanical properties of thin films of gold and silver, in *Structure and Properties of Thin Films*. John Wiley and Sons, New York 1959,183.
- (38) Hencky H. About the stress state in circular plates with negligible bending stiffness. *Z. Math. Phys* 1915, 63, 311.
- (39) Vlassak J.J. New experimental techniques and analysis methods for the study of mechanical properties of materials in small volumes. Ph.D. Dissertation, Stanford University 1994.
- (40) Levy S. Large deflection theory for rectangular plates, in *Non-linear Problems in Mechanics of Continua*, Appl. Math. I, Am. Math. Soc., New York 1949, 197.
- (41) Vlassak J.J; Nix W.D. A new bulge test technique for the determination of Young's modulus and Poisson's ratio of thin films. *J. Mater. Res* 1992, 7, 3242.

- (42) Timoshenko S.; Woinowsky K. S. Theory of Plates and Shells. McGraw-Hill, New York, 1959, 580
- (43) Itozaki H. Mechanical properties of composition modulated cop- per-palladium foils. Ph.D. Dissertation, Northwestern University, 1982.
- (44) Small M.K.; Nix W.D. Analysis of the accuracy of the bulge test in determining the mechanical properties of thin-films. J. Mater. Res 1992, 7, 1553.
- (45) Small M.K.; Vlassak J.J.; Nix W.D Re-examining the bulge test: Methods for improving accuracy and reliability, in Thin Films: Stresses and Mechanical Properties III, Mater. Res. Soc. Symp. Proc. 1992, 239, 257.
- (46) Xiang Y.; Chen X.; Vlassak J.J. Plane-strain bulge test for thin films. J Mater Res 2005, 20(9):2360–2370
- (47) Allen M.G.; Senturia S.D. Analysis of critical debonding pressures of stressed thin-films in the blister test. J Adhes 1988, 25(4):303–315
- (48) Williams J.G. Energy release rates for the peeling of flexible membranes and the analysis of blister tests. Int J Fract 1997, 87(3):265–288
- (49) Wan K.T.; Guo S.; Dillard D.A. A theoretical and numerical study of a thin clamped circular film under an external load in the presence of a tensile residual stress. Thin Solid Films 2003, 425(1–2):150–162
- (50) Gent A.N.; Lewandowski L.H. Blow-off pressures for adhering layers. J Appl Polym Sci 1987, 33(5):1567–1577
- (51) Tabata O.; Kawahata K.; Sugiyama S. Mechanical property measurements of thin films using load-deflection of composite rectangular membrane[C]//Micro Electro Mechanical Systems, 1989, Proceedings, An Investigation of Micro Structures, Sensors, Actuators, Machines and Robots. IEEE 1989, 152-156.
- (52) Kalkman A.J. A novel bulge-testing setup for rectangular free-standing thin films. Rev Sci Instrum 1999, (10):4026–4031
- (53) Xu D.W.; Liechti K.M.; de Lumley-Woodyear T.H. Closed form nonlinear analysis of the peninsula blister test. J Adhes 2006, 82 (8):831–866
- (54) Allen M.G. Micro fabricated structures for the insitu measurement of residual-stress, young's modulus, and ultimate strain of thin-films. Appl Phys Lett 1998, 51(4):241–243
- (55) Zheng D.W. Mechanical property measurement of thin polymeric-low dielectric-constant films using bulge testing method. Appl Phys Lett 2000, 76(15):2008–2010
- (56) Kalkman A.J.; Verbruggen A.H.; Janssen G. High temperature bulge-test setup for mechanical testing of freestanding thin films. Rev Sci Instrum 2003, 74(3):1383–1385

- (57) Schweitzer E.W.; Goken M. In situ bulge testing in an atomic force microscope: micro deformation experiments of thin film membranes. *J Mater Res* 2007, 22(10):2902–2911
- (58) Brust, M.; Walker, M.; Bethell, D.; Schiffrin, D. J.; Whyman, R. Synthesis of Thiol-Derivatised Gold Nanoparticles. *J. Chem. Soc., Chem. Commun.* 1994, 0, 801–802.
- (59) Holmberg, V. C.; Korgel, B. A. Corrosion Resistance of Thiol- and Alkene-Passivated Germanium Nanowires. *Chem. Mater.* 2010, 22, 3698–3703.